Applied Mathematics and Computation 310 (2017) 15–39

Contents lists available at ScienceDirect

Applied Mathematics and Computation

journal homepage: www.elsevier.com/locate/amc

Numerical investigation of electrohydrodynamic instability in a vertical porous layer

B.M. Shankar[a,*], Jai Kumar[b], I.S. Shivakumara[c]

[a] Department of Mathematics, PES University, Bangalore 560085, India
[b] ISRO Satellite Centre, Bangalore 560017, India
[c] Department of Mathematics, Bangalore University, Bangalore 560001, India

ARTICLE INFO

Keywords:
Electrohydrodynamic instability
Vertical porous layer
Chebyshev collocation method

ABSTRACT

The electrohydrodynamic instability of a vertical dielectric fluid saturated Brinkman porous layer whose vertical walls are maintained at different temperatures is considered. An external AC electric field is applied across the vertical porous layer to induce an unstably stratified electrical body force. The stability eigenvalue equation is solved numerically using the Chebyshev collocation method. The presence of inertia is found to instill instability on the system and the value of modified Darcy–Prandtl number Pr_D at which the transition from stationary to travelling-wave mode takes place is independent of the AC electric field but increases considerably with an increase in the value of Darcy number *Da*. The presence of AC electric field promotes instability but its effect is found to be only marginal. Although the flow is stabilizing against stationary disturbances with increasing *Da*, its effect is noted to be dual in nature if the instability is via travelling-wave mode. The streamlines and isotherms for various values of physical parameters at their critical state are presented and analyzed. Besides, energy norm at the critical state is also computed and found that the disturbance kinetic energy due to surface drag, viscous force and dielectrophoretic force have no significant effect on the stability of fluid flow.

1. Introduction

Natural convection in a layer of fluid saturated porous medium has constituted a pole of attraction to researchers because of its applications in several fields such as oil recovery, soil mechanics, rheology, metal casting, ceramic engineering, solid-matrix compact heat exchangers, spread of contaminants in the environment and in various processes in the chemical and materials industry, and the technologies of paper, textiles, insulating materials. Available works on this topic are concerned mostly with the study of natural convection in horizontal porous layers heated from below. The state of the art has been summarized in the books by Nield and Bejan [1] and Straughan [2,3].

The stability of natural convection in a vertical porous layer has been investigated by many authors. Gill [4] was the first to investigate the stability properties of natural convection in a vertical layer of Darcy porous medium and his findings established a rigorous ground for the use of insulating porous materials in buildings, instead of air gaps. Kwok and Chen [5] discussed different qualitative behaviors of the Darcy flow model used by Gill [4] considering the full Darcy–Brinkman model with advective inertia and also performed experiments. Qin and Kaloni [6] used energy methods to give

* Corresponding author.
E-mail addresses: bmshankar@pes.edu, shankarmahadev07@gmail.com (B.M. Shankar).

http://dx.doi.org/10.1016/j.amc.2017.04.032
0096-3003/

Nomenclature

a	vertical wave number
c	wave speed
c_r	phase velocity
c_i	growth rate
$D = d/dx$	differential operator
$Da = \mu_e K/\mu h^2$	Darcy number
$\vec{E}$	root-mean-square value of the electric field
E_b, E_d, E_D, E_e, E_s	disturbance kinetic energies
E_0	root-mean-square value of the electric field at $x = 0$
$\vec{f}_e$	force of electrical origin
$\vec{g}$	acceleration due to gravity
h	half- width of the porous layer
K	permeability
p	pressure
$P = p - 0.5\rho(\partial\varepsilon/\partial\rho)(\vec{E}\cdot\vec{E})$	modified pressure
$Pr_D = \nu h^2\varphi_p^2/K\kappa$	modified Darcy–Prandtl number
$\vec{q} = (u, v, w)$	velocity vector
$R_D = \alpha g\beta h^2 K/\nu\kappa$	Darcy–Rayleigh number
$R_{eaD} = \gamma^2\varepsilon_0 E_0^2\beta^2 h^2 K/\mu\kappa$	AC electric Darcy–Rayleigh number
t	time
T	temperature
T_c, T_d	disturbance thermal energies
T_1	temperature of the left vertical boundary
T_2	temperature of the right vertical boundary
V	root-mean-square value of the electric potential
V_1	electric potential of the left vertical boundary
V_2	electric potential of the right vertical boundary
W_b	basic velocity
(x, y, z)	Cartesian coordinates

Greek symbols

α	thermal expansion coefficient
$\beta = (T_2 - T_1)/h$	temperature gradient
γ	thermal expansion coefficient of dielectric constant
ε	dielectric constant
ε_0	reference dielectric constant at T_0
κ	thermal diffusivity
χ	ratio of heat capacities
μ	dynamic viscosity
μ_e	effective fluid viscosity
$\nu(=\mu/\rho_0)$	kinematic viscosity
$\psi(x, z, t)$	stream function
Ψ	amplitude of vertical component of perturbed velocity
ϕ	amplitude of perturbed electric potential
φ_p	porosity of the porous medium
ρ	fluid density
ρ_e	free charge density
ρ_0	reference density at T_0
σ	electrical conductivity of the fluid
θ	amplitude of perturbed temperature

sufficient conditions for the stability of convection in a vertical porous slab. Most of the developments are covered in the book by de Lemos [7]. Barletta [8] reconsidered Gill's problem and showed that the change of velocity boundary conditions from impermeable to permeable causes instability while Barletta [9] studied two-dimensional stationary mixed convection in a vertical porous layer. Rees [10] and Scott and Straughan [11] presented a new perspective on Gill's problem by taking into account of the local thermal nonequilibrium effect, while Shankar and Shivakumara [12,13] extended Gill's and Rees's problems for an Oldroyd-B type of viscoelastic fluid, respectively. Recently, the effect of inertia on the stability of

buoyancy-driven parallel shear flow in a vertical layer of isotropic and anisotropic porous medium using the Lapwood–Brinkman model is discussed by Shankar et al. [14,15].

The interaction between electric and/or magnetic field on fluid flow in a porous medium is of interest in many practical applications and is important particularly in the solidification process and geophysical context. Thermal convection in the presence of a uniform applied vertical magnetic field, known as magnetoconvection, has been investigated in a horizontal layer of porous medium in the past (Rudraiah [16], Alchaar et al. [17], Bergman et al. [18], Muddamallappa et al. [19], Bhatta et al. [20], Riahi [21]). The linear stability of plane-Poiseuille flow at high Reynolds numbers and in the presence of a transverse magnetic field is investigated theoretically using the multideck asymptotic approach by Makinde [22], while Makinde and Mhone [23] investigated the temporal stability of magnetohydrodynamic Jeffery–Hamel flows at very small magnetic Reynolds number. The Chebyshev spectral collocation method is employed to investigate the temporal development of small disturbances in a channel filled with a saturated porous medium under in the influence of magnetic field was studied by Makinde and Mhone [24]. Shankar et al. [25] examined magnetohydrodynamic stability of natural convection in a vertical porous slab. Electrohydrodynamics, coupling of the electric field and fluid motion, has led to many complex and interesting instability phenomena. Incipient interest in theoretical studies was limited to electrohydrodynamic(EHD) convection in a layer of dielectric fluid saturated porous medium caused by the dielectrophoretic force due to the variation in the dielectric constant with the non-homogeneous temperature gradient in the bulk flow (Moreno et al. [26], del Río and Whitaker [27], Rudraiah and Gayathri [28], Shivakumara et al. [29,30]). The effect of a uniform horizontal AC electric field on the stability of natural convection in a vertical dielectric fluid layer was examined by Takashima and Hambata [31] while the effect of a transverse uniform magnetic field on the stability of natural convection in a vertical layer of an electrically conducting fluid was analyzed by Takashima [32].

Nonetheless, studies pertaining to the stability of natural convection in a vertical dielectric fluid saturated porous layer under the influence of electric field have been almost completely neglected. Electrohydrodynamic coupled heat transfer in a fluid saturated vertical porous layer becomes important in geophysics to study the Earth's core and to understand the performance of petroleum reservoir. Moreover, the drying process in porous media is a rather complicated process as coupled heat and mass transport phenomena are involved simultaneously. Therefore, new techniques are being used to make the drying processes more efficient and one of the effective ways to improve the overall drying kinetics is to apply an electric field (Yabe et al. [33], Lai and Lai [34]). The foregoing observations provide the motivation to investigate the stability of natural convection in a vertical layer of dielectric fluid saturated Brinkman porous medium in the presence of a uniform horizontal AC electric field.

2. Mathematical formulation

The physical configuration of the problem is illustrated in Fig. 1. We consider a dielectric fluid saturated vertical layer of a porous medium confined between two parallel vertical plates at $x=\pm h$, subject to a uniform AC electric field applied across the vertical porous layer. The plate at $x=-h$ is maintained at fixed temperature T_1 and fixed electric potential $V_1(=0)$, while the plate at $x=h$ is maintained at fixed temperature $T_2(>T_1)$ and at an alternating (60 Hz) potential whose root-mean-square value is V_2. A Cartesian coordinate system (x, y, z) is chosen with the origin in the middle of the vertical porous layer, where the x-axis is taken perpendicular to the plates and the z-axis is vertically upwards, opposite in the direction of gravity. The relevant basic equations under the Oberbeck–Boussinesq approximation are ([1,31]):

$$\nabla\cdot\vec{q}=0 \tag{1}$$

$$\rho_0\left[\frac{1}{\varphi_p}\frac{\partial\vec{q}}{\partial t}+\frac{1}{\varphi_p^2}(\vec{q}\cdot\nabla)\vec{q}\right]=-\nabla p-\frac{\mu}{K}\vec{q}+\mu_e\nabla^2\vec{q}+\vec{f}_e+\rho\vec{g} \tag{2}$$

$$\chi\frac{\partial T}{\partial t}+(\vec{q}\cdot\nabla)T=\kappa\nabla^2T \tag{3}$$

$$\rho=\rho_0\{1-\alpha(T-T_0)\} \tag{4}$$

where $\vec{q}=(u,v,w)$ is the velocity vector, p is the pressure, ρ is the fluid density, $\vec{g}$ is the acceleration due to gravity, μ is the dynamic viscosity, μ_e the effective viscosity, K is the permeability, T is the temperature, φ_p is the porosity of the porous medium, χ is the ratio of heat capacities, κ is the thermal diffusivity, α is the thermal expansion coefficient, ρ_0 is the density at reference temperature $T=T_0=(T_1+T_2)/2$ and $\vec{f}_e$ is a body force term which represents the response of the fluid to the electric field and can be expressed as (Landau and Lifshitz [35])

$$\vec{f}_e=\rho_e\vec{E}-\frac{1}{2}\left(\vec{E}\cdot\vec{E}\right)\nabla\varepsilon+\frac{1}{2}\nabla\left(\rho\frac{\partial\varepsilon}{\partial\rho}\vec{E}\cdot\vec{E}\right) \tag{5}$$

Here $\vec{E}$ is the root-mean-square value of the electric field, ρ_e is the free charge density and ε is the dielectric constant. The electrical force $\vec{f}_e$ will have no effect on the bulk of the dielectric fluid if the dielectric constant ε and the electrical conductivity σ are homogeneous. Since ε and σ are functions of temperature, a temperature gradient applied to a dielectric

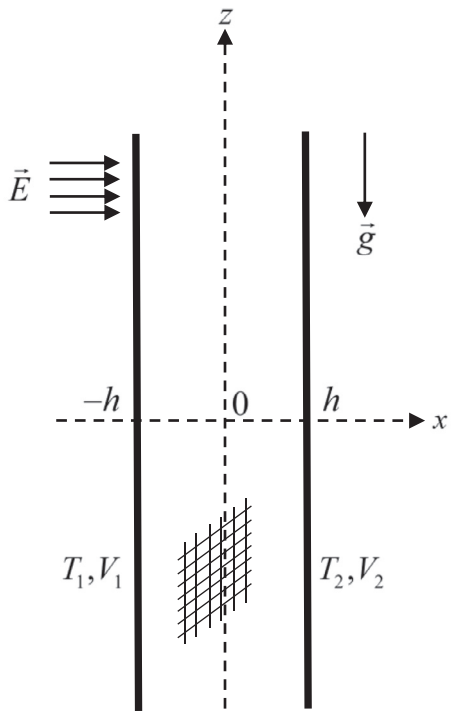

Fig. 1. Sketch of the porous channel (*xz*-plane section).

fluid produces a gradient in ε and σ. The application of DC electric field then results in the accumulation of free charge in the liquid. The free charge increases exponentially in time with a time constant ε/σ, which is known as the electrical relaxation time. If an AC electric field is applied at a frequency much higher than the reciprocal of the electrical relaxation time, the free charge does not have time to accumulate. Moreover, the electrical relaxation time of most dielectric liquids appear to be sufficiently long to prevent the buildup of free charge at standard power line frequencies. At the same time, dielectric loss at these frequencies is so low that it makes no significant contribution to the temperature field. The Coulomb force term $\rho_e\vec{E}$ in Eq. (5) is the force per unit volume on a medium containing free electric charge of density ρ_e. It is the strongest EHD force term and usually dominates when DC electric fields are present in dielectric fluids. The second term in Eq. (5), called dielectrophoretic force term, is due to the force exerted on a dielectric fluid by a nonuniform electric field. It is usually weaker than the free charge force term and only dominates when the AC electric field is imposed on a dielectric fluid. Therefore, the Coulomb force term has been neglected in Eq. (5) and only the dielectrophoretic force term is retained in Eq. (5). It is seen that the dielectrophoretic force term depends on $(\vec{E}\cdot\vec{E})$ rather than $\vec{E}$. Since the variation of $\vec{E}$ is very rapid, the root-mean-square value of $\vec{E}$ is used as the effective value in determining fluid motion. In other words, one can treat the AC electric field as the DC electric field whose strength is equal to the root-mean-square value of the AC electric field (Takashima and Aldridge [36]). The last term in Eq. (5) is called the electrostriction term. This term can be conveniently clubbed with the pressure in Eq. (5) and, because pressure amounts to an extra variable in incompressible flow, seems not to have any influence on the hydrodynamics.

Since there is no free charge, the relevant Maxwell equations are

$$\nabla\times\vec{E}=0,\quad \nabla\cdot(\varepsilon\vec{E})=0. \tag{6a,b}$$

In view of Eq. (6a), $\vec{E}$ can be expressed as

$$\vec{E}=-\nabla V \tag{7}$$

where V is the root-mean-square value of the electric potential. The dielectric constant is assumed to be a linear function of temperature in the form

$$\varepsilon=\varepsilon_0[1-\gamma(T-T_0)] \tag{8}$$

where $\gamma(>0)$ is the thermal expansion coefficient of dielectric constant and is assumed to be small. For example, for 10 cs Silicone oil $\gamma=2.86\times10^{-3}K^{-1}$ and $\varepsilon=2.6\times10^{-11}Fm^{-1}$.

3. Basic state

It is assumed that the basic steady-state flow is laminar and fully developed. Thus,

$$\vec{q} = W_b(x)\hat{k},\ P = P_b(x,z),\ \vec{E} = \vec{E}_b(x)\hat{i},\ T = T_b(x),\ \rho = \rho_b(x),\ \varepsilon = \varepsilon_b(x),\ V = V_b(x) \tag{9}$$

where the subscript b denotes the basic state. Under this circumstance, the basic state solution is found to be (Takashima and Hamabata [31])

$$W_b = \frac{\alpha g \beta K}{2\nu}\left[x - h\ \text{cosech}\left(\sqrt{\frac{\mu h^2}{\mu_e K}}\right)\sinh\left(x\sqrt{\frac{\mu h^2}{\mu_e K}}\right)\right] \tag{10}$$

$$P_b = \text{const} - \rho_0 g z + \frac{\varepsilon_0 E_0^2}{2(1-\gamma\beta x/2)} \tag{11}$$

$$T_b - T_0 = \beta x/2 \tag{12}$$

$$\rho_b = \rho_0\left(1 - \frac{\alpha\beta x}{2}\right) \tag{13}$$

$$\varepsilon_b = \varepsilon_0\left(1 - \frac{\gamma\beta x}{2}\right) \tag{14}$$

$$\vec{E}_b = \frac{E_0}{1-\gamma\beta x/2}\hat{i} \tag{15}$$

and hence

$$V_b = \frac{2E_0}{\gamma\beta}\log\left(\frac{1-\gamma\beta x/2}{1+\gamma\beta h/2}\right) \tag{16}$$

where

$$P = p - 0.5\rho(\partial\varepsilon/\partial\rho)\left(\vec{E}\cdot\vec{E}\right) \tag{17}$$

is the modified pressure and

$$E_0 = \frac{\gamma\beta V_2}{2}\log\left(\frac{1+\gamma\beta h/2}{1-\gamma\beta h/2}\right) \tag{18}$$

is the root-mean-square value of the electric field at $x=0$ and $\beta=(T_2-T_1)/h$ is the temperature gradient in the horizontal direction. Here, W_b and P_b have been determined under the condition that the total flux of flow across a horizontal plane z=constant is zero. It is observed that in the initial steady state the electric field does not affect the flow field.

4. Linear stability analysis

To study the linear stability of fluid flow, we superimpose an infinitesimal disturbance on the base flow in the form

$$\vec{q} = \vec{q}_b + \vec{q}',\ P = P_b(x,z) + P',\ V = V_b + V',\ T = T_b + T',\ \rho = \rho_b + \rho',\ \varepsilon = \varepsilon_b + \varepsilon'. \tag{19}$$

Substituting Eq. (19) into Eqs. (1)–(3), linearizing by neglecting the product of perturbed quantities, we get

$$\nabla\cdot\vec{q}' = 0 \tag{20}$$

$$\frac{1}{\varphi_p}\frac{\partial\vec{q}'}{\partial t} + \frac{1}{\varphi_p^2}\left\{(\vec{q}_b\cdot\nabla)\vec{q}' + \left(\vec{q}'\cdot\nabla\right)\vec{q}_b\right\} = -\frac{1}{\rho_0}\nabla P' - \frac{1}{\rho_0}\left(\frac{\mu}{K} - \mu_e\nabla^2\right)\vec{q}' + \alpha T' g\hat{k} - \frac{E_0\gamma\beta\varepsilon_0}{2\rho_0}\frac{\partial V'}{\partial x}\hat{i} - \frac{E_0^2\gamma^2\beta\varepsilon_0}{2\rho_0}T'\hat{i} \tag{21}$$

$$\chi\frac{\partial T'}{\partial t} + (\vec{q}_b\cdot\nabla)\vec{q}' + (\vec{q}'\cdot\nabla)T_b = \kappa\nabla^2 T' \tag{22}$$

$$\gamma E_0\frac{\partial T'}{\partial x} = -\nabla^2 V'. \tag{23}$$

We restrict our attention to two-dimensional disturbances (Squire's theorem provides justification for working in two dimensions rather than three dimensions [37]) and the resulting equations are made dimensionless by scaling (x, y, z) by h, t by $\varphi_p h^2/\kappa$, $\vec{q}'$ by κ/h, T' by βh, V' by $\gamma\beta E_0 h^2$ and P' by $\kappa\mu/hK$ to get (after discarding the primes for simplicity)

$$\frac{\partial u}{\partial x}+\frac{\partial w}{\partial z}=0 \tag{24}$$

$$\frac{1}{Pr_D}\left(\frac{\partial u}{\partial t}+W_b\frac{\partial u}{\partial z}\right)=-\frac{\partial P}{\partial x}-u+Da\left(\frac{\partial^2 u}{\partial x^2}+\frac{\partial^2 u}{\partial z^2}\right)-\frac{R_{eaD}}{2}\left(\frac{\partial V}{\partial x}+T\right) \tag{25}$$

$$\frac{1}{Pr_D}\left(\frac{\partial w}{\partial t}+u\,DW_b+W_b\frac{\partial w}{\partial z}\right)=-\frac{\partial P}{\partial z}-w+Da\left(\frac{\partial^2 w}{\partial x^2}+\frac{\partial^2 w}{\partial z^2}\right)+R_D T \tag{26}$$

$$M\frac{\partial T}{\partial t}+W_b\frac{\partial T}{\partial z}+\frac{u}{2}=\frac{\partial^2 T}{\partial x^2}+\frac{\partial^2 T}{\partial z^2} \tag{27}$$

$$\frac{\partial T}{\partial x}=-\left(\frac{\partial^2 V}{\partial x^2}+\frac{\partial^2 V}{\partial z^2}\right) \tag{28}$$

where $D=d/dx$, $R_{eaD}=\gamma^2\varepsilon_0 E_0^2\beta^2 h^2 K/\mu\kappa$ is the AC electric Darcy-Rayleigh number, $Pr_D=\nu h^2\varphi_p^2/K\kappa$ is the modified Darcy–Prandtl number, $R_D=\alpha g\beta h^2 K/\nu\kappa$ is the Darcy–Rayleigh number, $Da=\mu_e K/\mu h^2$ is the Darcy number, and $M=\chi/\varphi_p$. It should be noted that the basic velocity in dimensionless form is

$$W_b=\frac{R_D}{2}\left[x-\operatorname{cosech}\left(Da^{-1/2}\right)\sinh\left(Da^{-1/2}x\right)\right]. \tag{29}$$

Eliminating the pressure P from the momentum equations, introducing a stream function $\psi(x, z, t)$ through

$$u=\frac{\partial\psi}{\partial z}, w=-\frac{\partial\psi}{\partial x} \tag{30}$$

and employing the normal mode analysis procedure in the form

$$\{\psi, T, V\}=\{\Psi,\theta,\phi\}(x)e^{ia(z-ct)} \tag{31}$$

where c is the wave speed which is real and positive and a is the vertical wave number, we obtain

$$\frac{1}{Pr_D}\left[(W_b-c)\left(D^2-a^2\right)\Psi-D^2W_B\Psi\right]+\frac{R_{eaD}}{2}(D\phi+\theta)=\frac{1}{ia}\left[Da\left(D^2-a^2\right)^2\Psi-\left(D^2-a^2\right)\Psi-R_D D\theta\right] \tag{32}$$

$$(W_b-Mc)\theta+\frac{1}{2}\Psi=\frac{1}{ia}(D^2-a^2)\theta \tag{33}$$

$$D\theta+\left(D^2-a^2\right)\phi=0 \tag{34}$$

In general, $c=c_r+ic_i$ where c_r is the phase velocity and c_i is the growth rate. It is considered that on the rigid and isothermal vertical plates the tangential electric field vanishes. Thus the associated boundary conditions are:

$$\Psi=D\Psi=\theta=\phi=0 \quad \text{at } x=\pm1. \tag{35}$$

Eqs. (32)–(35) constitute a stability eigenvalue problem which is solved numerically by the well known Chebyshev collocation method (Orszag [38], Canuto et al. [39]). Accordingly, the field variables Ψ, θ and ϕ are approximated in terms of Chebyshev polynomials in the form

$$\Psi(x)=\sum_{j=0}^{N}\xi_j(x)\Psi_j,\quad \theta(x)=\sum_{j=0}^{N}\xi_j(x)\theta_j,\quad \phi(x)=\sum_{j=0}^{N}\xi_j(x)\phi_j \tag{36}$$

where $\xi_j(x)=\cos\ (j\cos^{-1}x)$. The usual procedure leads to the following generalized matrix eigenvalue problem (for details see Shankar et al. [40])

$$AX=cBX \tag{37}$$

where c is the eigenvalue and X is the discrete representation of the eigenfunction; A and B are square (complex) matrices of order 3(N+1). The eigenvalues and the eigenfunctions of the above matrix eigenvalue problem are determined with the aid of a QZ-algorithm which is available in the MATLAB software package in the form of built in function eig().

Table 1
Convergence of the Chebyshev collocation method.

N	$R_D = 20000, Pr_D = 5, R_{eaD} = 20, \sqrt{Da^{-1}} = 0.5, a = 1 = M$		$R_D = 20000, Pr_D = 20, R_{eaD} = 20, \sqrt{Da^{-1}} = 0.5, a = 1 = M$	
	c_r	c_i	c_r	c_i
1	−12.19739532	125.79237869	−0.00406956	138.33800182
5	−1.56843935	150.91954455	−6.81251762	161.64109986
10	−1.68402373	150.32443549	−6.83280114	161.66535648
15	−1.57766246	150.30126741	−6.77356582	161.62841441
20	−1.57748620	150.30259469	−6.77304924	161.62926681
25	−1.57746745	150.30253403	−6.77304791	161.62922607
30	−1.57746867	150.30253184	−6.77304971	161.62922666
35	−1.57746862	150.30253133	−6.77304969	161.62922662
40	−1.57746862	150.30253134	−6.77304968	161.62922660
50	−1.57746863	150. 30253133	−6.77304967	161.62922660
60	−1.57746862	150. 30253133	−6.77304968	161.62922660
70	−1.57746862	150. 30253133	−6.77304968	161.62922661
N	$R_D = 20000, Pr_D = 20, R_{eaD} = 20, \sqrt{Da^{-1}} = 1 = a = M$		$R_D = 20000, Pr_D = 20, R_{eaD} = 70, \sqrt{Da^{-1}} = 1 = a = M$	
	c_r	c_i	c_r	c_i
1	−46.88995317	378.65934057	−46.91487760	378.61382378
5	−8.59633138	539.87446855	−8.60038554	539.86143015
10	−5.42388056	545.87106826	−5.42352315	545.85900275
15	−8.80758431	543.99719042	−8.80801272	543.98425343
20	−8.98798858	543.97439971	−8.97846256	543.96249464
25	−8.98843536	543.97526623	−8.97890630	543.96251398
30	−8.98844532	543.97526400	−8.97890742	543.95252197
35	−8.98844548	543.97526048	−8.97890759	543.95252124
40	−8.98844542	543.97526041	−8.97890758	543.95252126
50	−8.98844542	543.97526041	−8.97890755	543.95252126
60	−8.98844541	543.97526040	−8.97890755	543.95252125
70	−8.98844542	543.97526041	−8.97890755	543.95252126

Table 2
Comparison of critical stability parameters.

$\sqrt{Da^{-1}}$	Makinde [41]			Present work		
	Re_c	α_c	c_c	Re_c	α_c	c_c
0	5772.2283	1.02052	0.263997	5772.267785	1.020	0.26352965
0.1	5832.2973	1.01986	0.262559	5831.536366	1.019	0.26240273
0.2	6015.0334	1.01781	0.258313	6014.402939	1.017	0.25815868
0.3	6328.7057	1.01492	0.251535	6328.339172	1.014	0.25136095
0.4	6787.3070	1.01074	0.242499	6787.228187	1.011	0.24233670
0.5	7411.1295	1.00561	0.231650	7411.468698	1.006	0.23149161
0.6	8227.4284	0.99966	0.219445	8228.361884	0.998	0.21927310
0.7	9271.2789	0.99307	0.206344	9273.216864	0.992	0.20613269
0.8	10586.3898	0.98608	0.192782	10589.39436	0.985	0.19258345

5. Energy norm at critical state

In order to understand the physical mechanism during the flow transition, it is necessary to define an inner-product and the associated norm. This will allow one to address the orthogonality of the eigenfunctions as well as the size of perturbations. For the temporal evolution of disturbances in an incompressible flow, the energy density of a disturbance is a physically meaningful measure of the size of the perturbation. The rate of change of two-dimensional (non dimensional) kinetic and thermal energies are given by

$$\frac{1}{Pr_D}\frac{\partial}{\partial t}\left\langle \frac{1}{2}\left(u^2+w^2\right)\right\rangle = -\frac{1}{Pr_D}\langle uwDW_b\rangle + R_D\langle wT\rangle - \left\langle u^2+w^2\right\rangle - Da\left\langle (\nabla u)^2 + (\nabla w)^2\right\rangle - \frac{R_{eaD}}{2}\left\langle u\frac{\partial V}{\partial x} + uT\right\rangle$$
$$= E_s + E_b + E_D + E_d + E_e \tag{38}$$

$$\frac{1}{2}\left\langle M\frac{\partial\left(T^2\right)}{\partial t}\right\rangle = -\frac{1}{2}\langle uT\rangle - \left\langle (\nabla T)^2\right\rangle = T_c + T_d \tag{39}$$

Table 3
Comparison of Chebyshev collocation and Galerkin method for different values of Pr_D and $\sqrt{Da^{-1}}$ when $R_{eaD}=50$ and $M=1$.

$\sqrt{Da^{-1}}$	Pr_D	Chebyshev collocation method			Galerkin method		
		R_{Dc}	a_c	c_c	R_{Dc}	a_c	c_c
0.5	1	16567.548915	1.374	0	16565.161995	1.371	0
	5	25881.212807	0.718	±196.269020	25885.1639271	0.714	±195.027960
	10	26789.475313	1.068	±207.938936	26784.973353	1.068	±206.329768
	50	55356.729218	1.274	±446.562448	55351.251781	1.269	±442.734840
	100	79604.651063	1.313	±647.255100	79607.009146	1.311	±644.656020
	200	115498.702807	1.323	±944.519679	115499.404833	1.323	±945.759288
1.0	1	1209.277224	1.363	0	1207.232984	1.362	0
	5	6040.636461	1.342	0	6044.601215	1.339	0
	10	12102.045597	1.342	0	12108.966391	1.339	0
	50	8161.211361	1.109	±238.188553	8165.156269	1.112	±237.590501
	100	11065.889915	1.206	±328.681413	11061.509310	1.201	±325.499233
	200	15656.609942	1.274	±470.376116	15654.645291	1.271	±469.698456
4.0	1	30.694852	0.934	0	30.099528	0.933	0
	5	254.972191	0.807	0	253.971346	0.810	0
	10	523.163845	0.780	0	521.133746	0.783	0
	50	2713.021507	0.792	0	2716.166397	0.791	0
	100	5441.506959	0.792	0	5447.608054	0.789	0
	200	2091.925568	0.718	±407.317435	2093.634812	0.719	±407.402539

where the brackets $\langle\rangle$ represent the volumetric average over the volume of disturbance waves. In Eq. (38), the first term on the right hand side, E_s represents the gain (loss) of the disturbance kinetic energy from (to) the mean flow through Reynolds stress, and is referred to the shear production (destruction). The term denoted by E_b is due to non-isothermal effects and represents the production (destruction) of disturbance kinetic energy through the buoyancy effect. The third, fourth and fifth terms (E_D, E_d and E_e) represent, respectively, the dissipation of disturbance kinetic energy due to surface drag, viscous force and electric force. The first term in E_e has cropped up due to non-uniform variation in the electric field and the second term is occurred due to dielectrophoretic forces caused by the variation in dielectric constant with the non-homogeneous temperature gradient in the bulk flow. In Eq. (39), quantities termed T_c and T_d are associated with disturbance thermal energy due to thermal convection and disturbance thermal energy due to diffusion effect. All derivatives are approximated by fourth-order finite difference in the given domain except at boundaries. Integrals are calculated using fourth-order Simpson's extended rule.

6. Results and discussion

The stability of natural convection in a vertical dielectric fluid saturated Brinkman porous layer under a uniform horizontal AC electric field is investigated numerically using the Chebyshev collocation method. The non-dimensional parameters involved in the present study are the Darcy-Rayleigh number R_D, AC electric Darcy-Rayleigh number R_{eaD}, Darcy number Da, Darcy-Prandtl number Pr_D and the non-dimensional group M. Convergence of the results is tested for different sets of parametric values by varying the order of base polynomial N (see Table 1). From the table it is evident that four digits point accuracy can be achieved by retaining 31 terms in Eq. (36). As the number of terms increased in Eq. (36), the results are found to remain consistent and the accuracy improved up to 5 digits for $N=30$ and up to 7 digits for $N=50$. The results presented here are for $N=50$. The results obtained in the absence of AC electric field are compared with those of isothermal porous channel flows as the numerical results are lacking for non-isothermal case in the open literature. The results so obtained for different values of Darcy number with proper adjustment of parameters are compared with those of Makinde [41] in Table 2 and note that there is a good agreement between them. The result corresponds to the nonporous domain case ($Da^{-1}=0$) is in conformity with the one obtained by Orszag [38]. Moreover, the eigenvalue problem is also solved numerically using the Galerkin method with Legendre polynomials as trial functions

$$\Psi(x)=\sum_{n=0}^{N} a_n(1-x^2)^2P_n(x),\ \theta(x)=\sum_{n=0}^{N} b_n(1-x^2)P_n(x),\ \phi(x)=\sum_{n=0}^{N} c_n\left(1-x^2\right)P_n(x)$$

where $P_n(x)$ is the Legendre polynomial of degree n and a_n, b_n and c_n are constants (Singer et al. [42], Chen and Chung [43]). The results obtained for a representative set of parametric values considering 55 terms in the Galerkin expansion are shown in Table 3 along with those obtained from the Chebyshev collocation method. It is seen that the results complement with each other.

The basic natural convection flow, stationary and parallel, is not influenced by the AC electric field. Nonetheless, the Darcy number and the Darcy-Rayleigh number influence the base flow significantly. Fig. 2(a) and (b) show the influence of Da^{-1} (with $R_D=2000$) and R_D (with $Da^{-1}=1$) on the basic velocity W_b, respectively. These figures indicate that the velocity

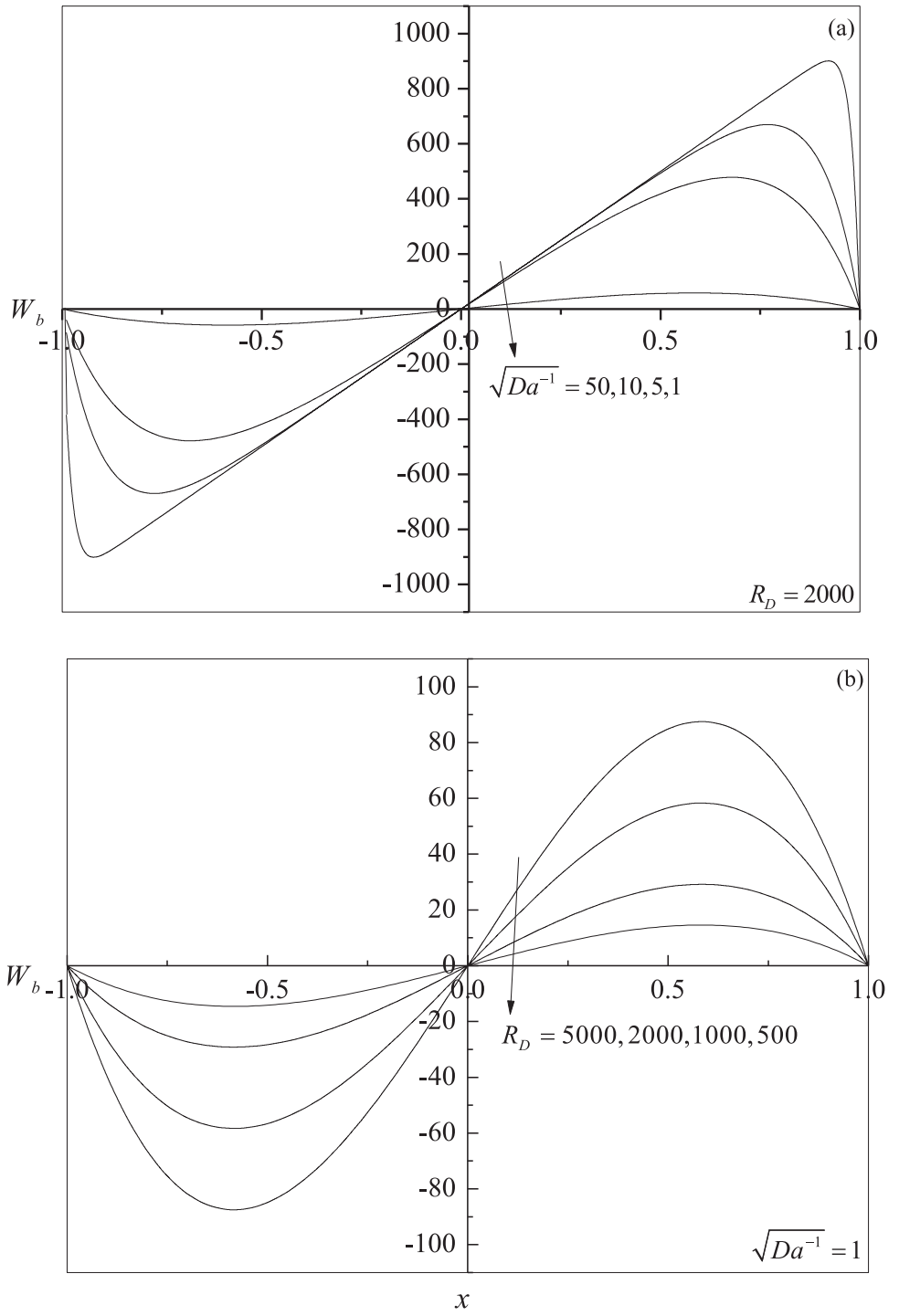

Fig. 2. Basic velocity profiles.

profiles are anti-symmetric about the vertical line at $x=0$ but they are not precisely centro-symmetric about $x=\pm 1/2$. In other words, in the half region, the basic velocity is in one direction and in the other half it is in the opposite direction and it is zero at $x=0$. Moreover, decrease in Da^{-1} is to suppress the fluid flow (Fig. 2(a)) and a similar trend is noticed with decreasing R_D (Fig. 2(b)). Also, at higher values of Da^{-1} we recover the Darcy flow case with a linear profile, but with thin boundary layers near the two vertical walls in order to satisfy the no-slip condition.

It is inquisitive to look at the results obtained under the limiting cases of $R_{eaD}=0$ (absence of electric field), $Pr_D \to \infty$ (absence of inertial effects) and $Da=0$ (Darcy case) as this problem was originally discussed analytically by Gill [4]. The

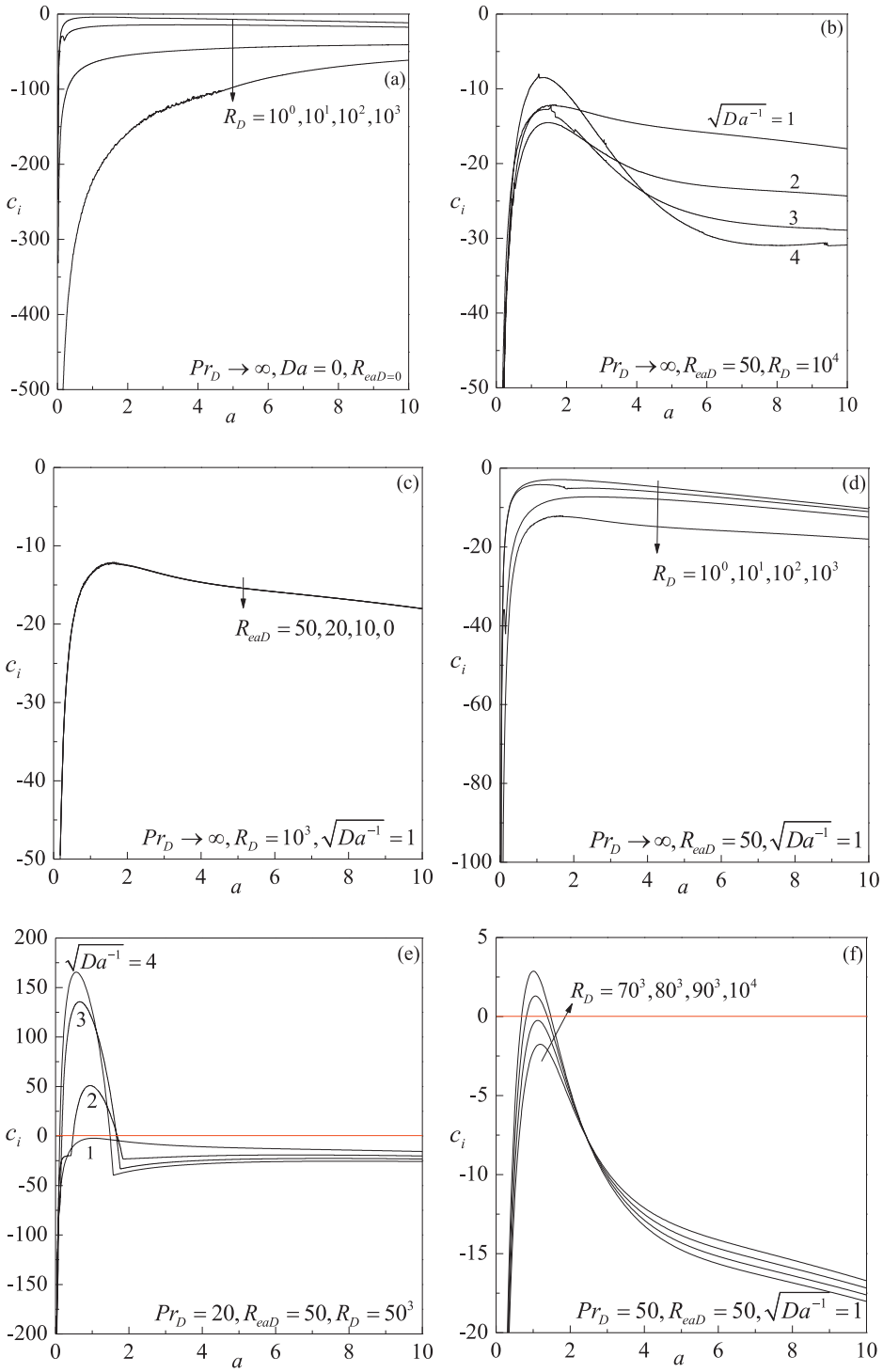

Fig. 3. Variation of growth rate c_i with wave number a.

overall trend displayed in Fig. 3(a) for this case shows the stability of the basic flow for all considered values of R_D which corroborate the results of Gill [4]. The basic flow is found to be stable even with the inclusion of Brinkman term and AC electric field when $Pr_D \to \infty$, and the results shown in Fig. 3(b)–(d) demonstrate that the equilibrium is always stable. Nonetheless, the study evidences an unstable behavior ($c_i > 0$) once the inertial effects are taken into consideration and this fact is evident from Fig. 3(e)–(h). A closer look at these figures reveals that there exists a threshold value of Da^{-1}, R_D

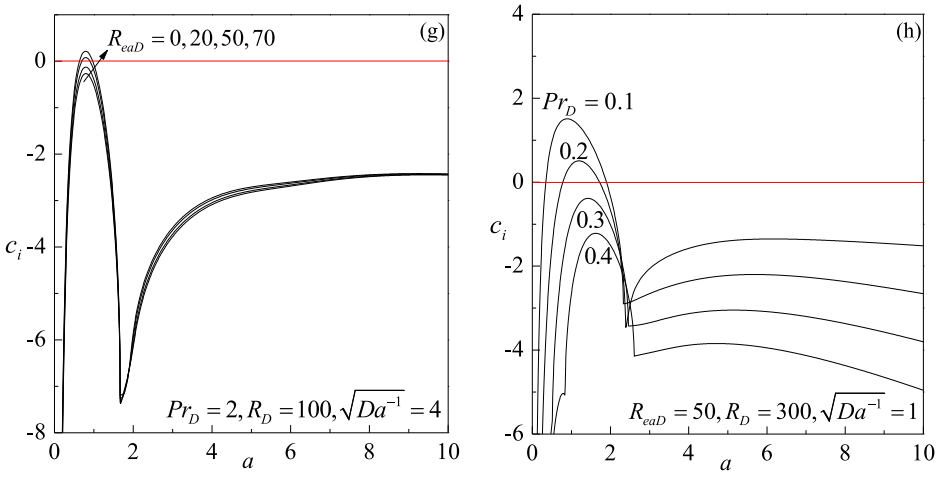

Fig. 3. Continued

and R_{eaD} above which (Fig. 3(e)–(g)), and the value of Pr_D below which (Fig. 3(h)) instability occurs. Moreover, the threshold values are interdependent on the parametric values involved therein.

Fig. 4(a)–(c) exhibit neutral stability curves in the (R_D,a)- plane for various values of Pr_D (with $Da^{-1}=16$, $R_{eaD}=50$), Da^{-1} (with $Pr_D=10$, $R_{eaD}=50$) and R_{eaD} (with $Pr_D=10$, $Da^{-1}=9$), respectively. The neutral stability curves exhibit single but different minimum with respect to the wave number for various values of Pr_D, Da^{-1} and R_{eaD} considered. The stability to linear perturbations corresponds to the region below and outside the neutral stability curves while the instability corresponds to the region above as well as inside each neutral stability curve. For the considered parametric values, Fig. 4(a) illustrates that there exists a threshold value of Pr_D(=136.9) below which the instability always occurs as stationary mode while beyond this threshold value the instability first occurs as a travelling-wave mode and switches over to stationary mode with further increase in the value of wave number. Despite the change of instability with increasing wave number, the travelling-wave mode turns out to be the preferred mode of instability. Moreover, it is seen that Pr_D exhibits a dual behavior on the stability of the basic flow depending on the mode of instability. Increasing Da^{-1} is to decrease the region of stability (Fig. 4(b)) and similar is the case with increasing R_{eaD} (Fig. 4(c)).

The variation of R_{Dc} and a_c as a function of Pr_D is illustrated in Fig. 5(a) and (b), respectively for different values of Da^{-1} when $R_{eaD}=50$ and $M=1$. Fig. 5(a) clearly indicates the existence of a threshold value of Pr_D at which the instability switches over from stationary to travelling-wave mode. Moreover, the threshold value of Pr_D increases significantly with increasing Da^{-1}. The effect of increasing Da^{-1} is to reinforce instability on the system. In other words, increasing Da^{-1} is to destabilize the basic flow if the instability is via stationary mode. This may be attributed to the fact that decreasing Darcy number is equivalent to decrease in the ratio of viscosities, μ_e/μ and hence its effect is to destabilize the system due to decrease in the viscous diffusion. However, when the instability is via travelling-wave mode the observed scenario is quite different. For this case, R_{Dc} passes through a minimum with increasing Pr_D up to a certain value of Da^{-1} and this trend eventually goes on diminishing with increasing Da^{-1} (= 4, 9, 16) and leading to instability of the system with Pr_D. The vertical lines represent the discontinuous changes in the critical wave number a_c due to the transition from stationary to travelling-wave mode (Fig. 5(b)). The figure indicates that the dependence of a_c on Pr_D is weak at stationary mode, whereas at travelling-wave mode a_c depends strongly on Pr_D. Also, the effect of increasing Da^{-1} is to enlarge the size of convection cells at both stationary and travelling-wave modes. The results of travelling-wave mode instability summarized in Fig. 5(c) indeed confirm the above observed behavior more evidently, which shows the variation of positive c_c with Pr_D for various values of Da^{-1}. The discontinuous changes in c_c due to the transition from stationary ($c_c=0$) to travelling-wave ($c_c \neq 0$) mode are represented by the vertical lines. From Fig. 5(c) it is observed that for values of $Da^{-1}=0.04$, 0.25 and 1, c_c values pass through a minimum with increasing Pr_D. This trend goes on diminishing with increasing Da^{-1} and for values of $Da^{-1}=4$, 9 and 16 the critical wave speed decreases with increasing Pr_D.

Fig. 6 shows the instability map on the (Pr_{DT},Da^{-1})-plane showing the division of the plane into zones of stationary and travelling wave modes. It is evident that the threshold value of the modified Darcy-Prandtl number at which the transition from stationary mode to travelling-wave mode occurs increases significantly with Da^{-1}.

The above observed facts are also viewed and analyzed through streamlines and isotherms at the critical state. In all the contour plots, dashed lines denote negative values whereas solid lines stand for positive values. In addition, for stream function, solid and dashed lines are associated with a clockwise and counter-clockwise rotation, respectively. Figs. 7 and 8 exhibit streamlines and isotherms before and after the transition mode as a function of Pr_D for $Da^{-1}=1=M$ and $R_{eaD}=50$. For $Pr_D=12.1$, the flow pattern appears to be as stationary and uni-cellular. Further, a closer look at the stream line contour shows that uni-cellular pattern moving alternatively clockwise and anti-clockwise along the z direction (Fig. 7(a)). The

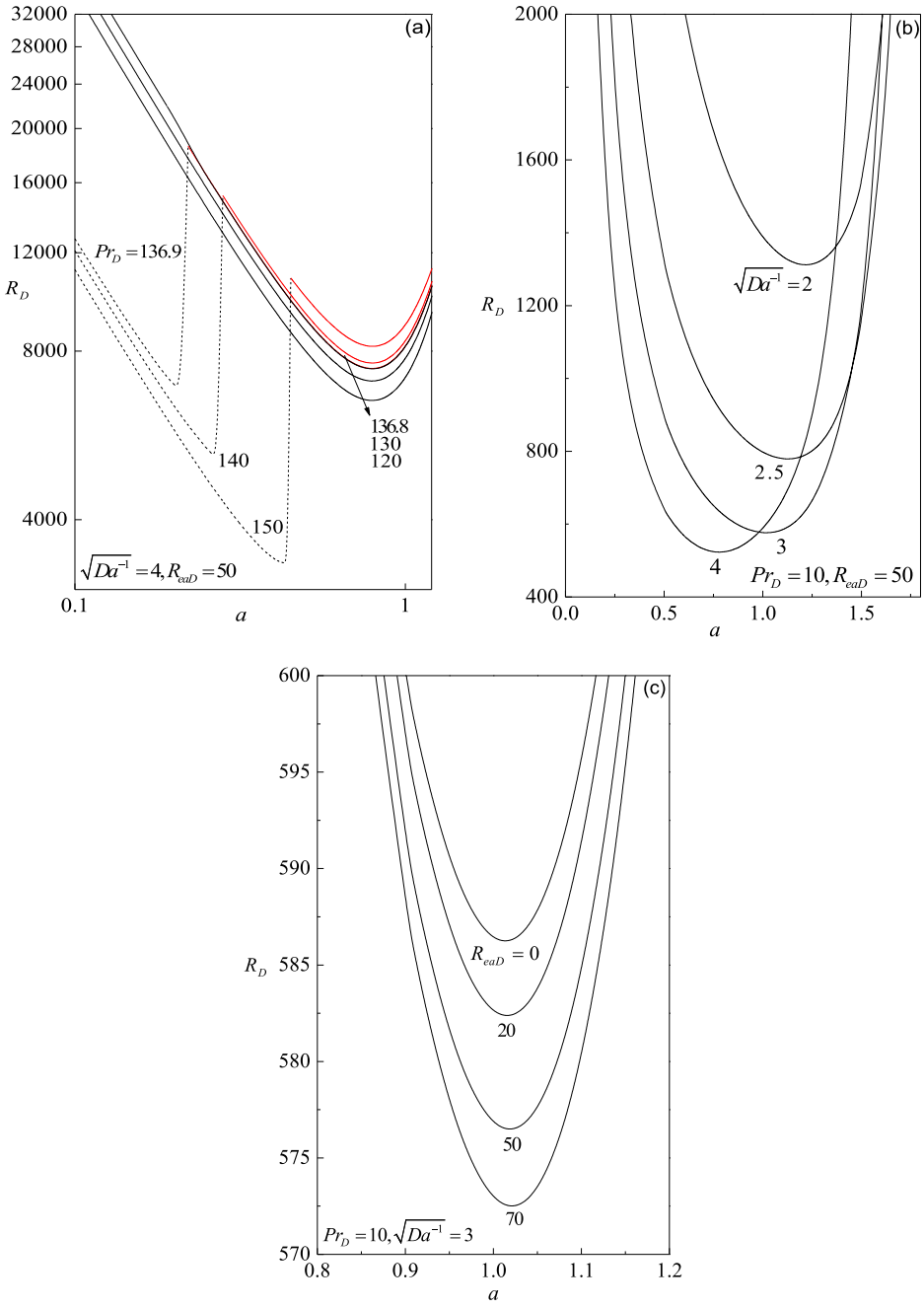

Fig. 4. Neutral stability curves for different values of Pr_D, $\sqrt{Da^{-1}}$ and R_{eaD} when $M = 1$. (——) Stationary modes, (.....) travelling-wave modes.

isotherms are uni-cellular and concentrate in the vicinity of the hot wall and which is evident from Fig. 8(a). The flow pattern and flow strength changes qualitatively as well as quantitatively as the mode of instability changes from stationary to travelling-wave with increasing Pr_D. In other words, the instability switches over from stationary to travelling-wave mode once the value of Pr_D exceeds the value 12.1. When $Pr_D = 12.3$, it is observed that the convective motion is constructed by two parts, one is the vigorous cell in the right half of the porous layer adjacent to the right surface, the other is the weak circulation which is exterior to the vigorous convection cell in streamlines (Fig. 7(b)). Also, shapes of the isotherms change (Fig. 8(b)). It is further seen that the actual wavelengths are substantially larger in both streamlines and isotherms and at this stage $\Psi_{\max}$ increases from 0.62 to 1.05, also $\theta_{\max}$ changes from 0.017 to 0.004. This fact is also evident from Figs. 7(b) and 8(b). Further increase in Pr_D is to decrease the wavelength as well as to increase the flow strength slightly (Fig. 7(c) and (d)) and also to strengthen the isotherms (Fig. 8(c) and (d)). From these figures, it is noted that the streamlines move closer

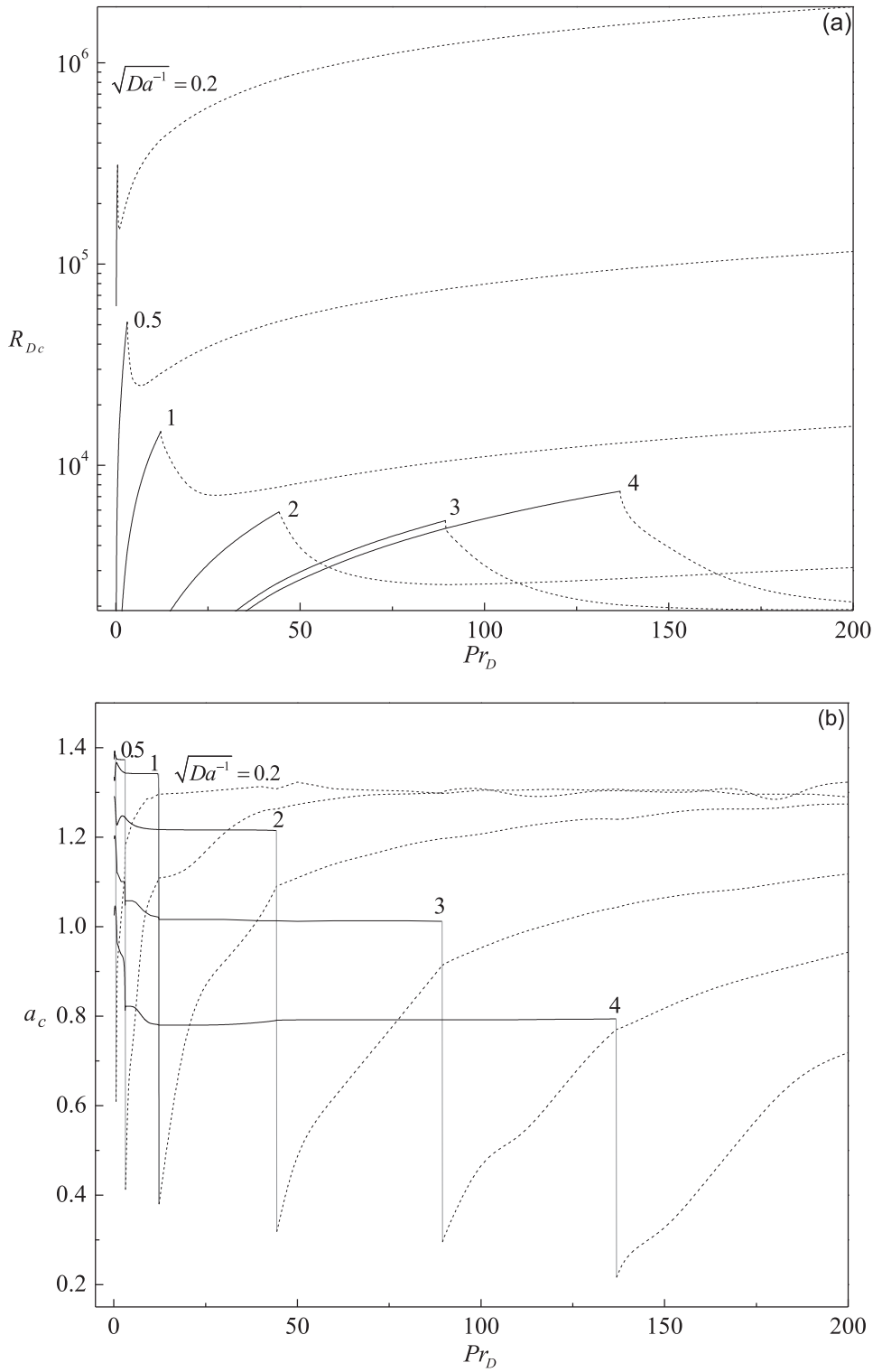

Fig. 5. Variation of (a) critical Darcy–Rayleigh number R_{Dc}, (b) critical wave number a_c and (c) critical wave speed c_c with the Darcy–Prandtl number Pr_D for a fixed value of $R_{eaD} = 50$, $M = 1$ and for various values of $\sqrt{Da^{-1}}$. (——) Stationary modes, (.....) travelling-wave modes.

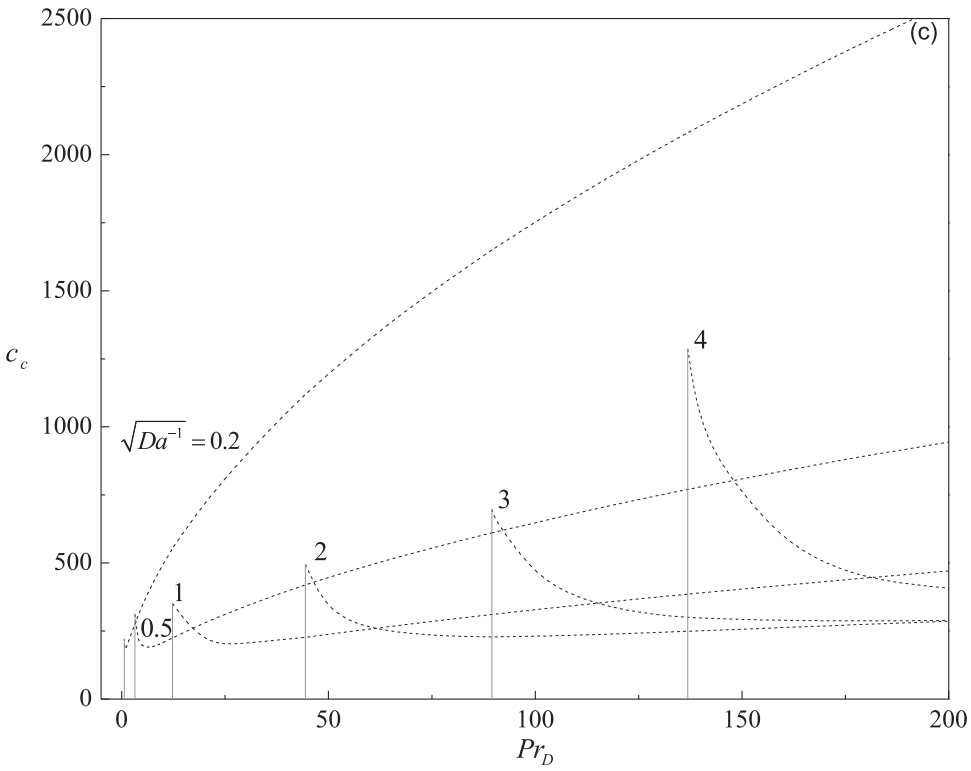

Fig. 5. Continued

and appear to be parallel at the center of the vertical fluid-saturated porous layer and bi-cellular oblate triangles occupy the whole thickness of the vertical porous layer in isotherms. With increasing Pr_D (136.7 and 136.9), it is observed that the magnitude of secondary flow changes in both streamlines and isotherms (Figs. 7(e), (f) and 8(e), (f)).

To know the impact of Darcy number on the stability characteristics of the system, the results are presented for $Da^{-1}=4$ in Fig. 9. The streamlines and isotherms are shown in Fig. 9(a, b) and (c, d), respectively, for $Pr_D=44.2$ and 44.4. For $Pr_D=44.2$, the pattern appears to be stationary unicellular both in streamlines and isotherms (Fig. 9(a) and (c)). As Pr_D increases to 44.4 (Fig. 9(b)), a sudden change in the magnitude of secondary flow is observed (i.e., $\Psi_{\max}=0.63$ to 1.11) and convective cells transform from unicellular to bi-cellular in streamlines. In the case of isotherms, as mode changes from stationary to travelling-wave, the magnitude of isothermal lines reduce drastically ($\theta_{\max}=0.02$ to 0.003). Also, shapes of the isotherms change from unicellular to multi-cellular (Fig. 9(d)). This behavior of the streamlines and isotherms may be due to the change in the mode of instability from stationary to travelling-wave mode.

To get a clear understanding about the characteristics of neutral stability of fluid flow for a given set of parameters, energy spectrums of the secondary flow are analyzed in detail. Theoretically at the critical points, $\partial E_{kin}/\partial t=0$ and $\partial E_{thm}/\partial t=0$. In other words, total kinetic energy (E_{kin}) as well as thermal energy (E_{thm}) production must balance the energy dissipation. In all the numerical results produced here for energy analysis, this phenomenon is observed at the critical points.

The neutral stability curves of the given flow show that the threshold value of Pr_D, where the secondary flow changes its mode from stationary to travelling-wave mode, is a strong function of Da^{-1}. For understanding this phenomenon, variation of kinetic and thermal energy components are analyzed as a function of Pr_D and shown in Figs. 10–12 for three different values of $Da^{-1}=0.25$, 1 and 4, respectively, for a fixed value of $R_{eaD}=50$ and M = 1. It can be seen that for $Da^{-1}=0.25$, shear production (E_s) has a tendency to destabilize the flow and viscous dissipation (E_d) stabilizes it, in the domain [0.1, 3] of Pr_D. However, the contribution of energy production due to buoyancy term (E_b) is not negligible in this domain. Quantitatively, in this domain contribution of shear and buoyant term is around 80 and 20% approximately in the instability of flow, respectively. Furthermore, the production of kinetic energy due to shear term diminishes drastically as Pr_D changes from 3.0 to 3.1, which could be associated to the change of stationary to travelling-wave mode of secondary flow. After this threshold value of Pr_D (= 3), E_d is responsible to stabilize the flow and buoyant instability (E_b) is the only instability mode. For this range of Pr_D(> 3.1), other components of kinetic energy have negligible influence on the stability or instability of the flow. However, a sudden change in the role of components of kinetic energy is observed for the value of Pr_D *at which* the mode of instability changes. Another important observation here is that the total kinetic energy production is almost balanced by energy dissipation due to viscous force term (E_d) in the entire domain of modified Darcy–Prandtl number (Fig. 10a). From Figs. 11(a) and 12(a), it can be concluded that, for $Da^{-1}=1$ and 4 also kinetic energy spectrums show a similar character-

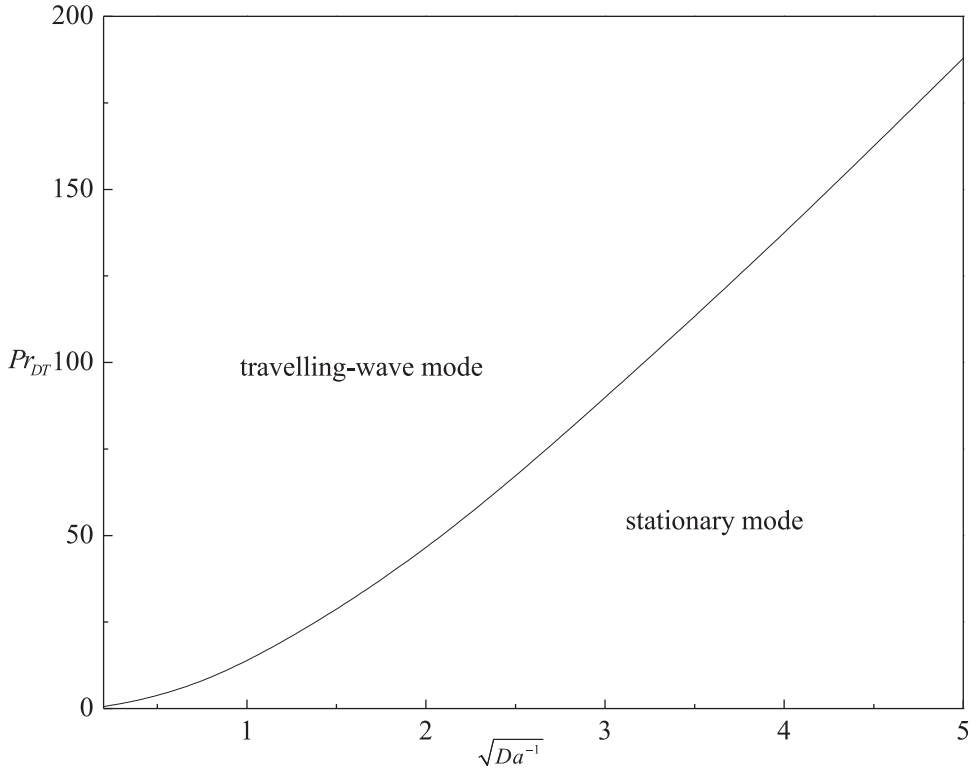

Fig. 6. Variation of Pr_{DT} (transition Darcy–Prandtl number at the critical domains) as a function of $\sqrt{Da^{-1}}$ when $R_{eaD}=50$, $M=1$.

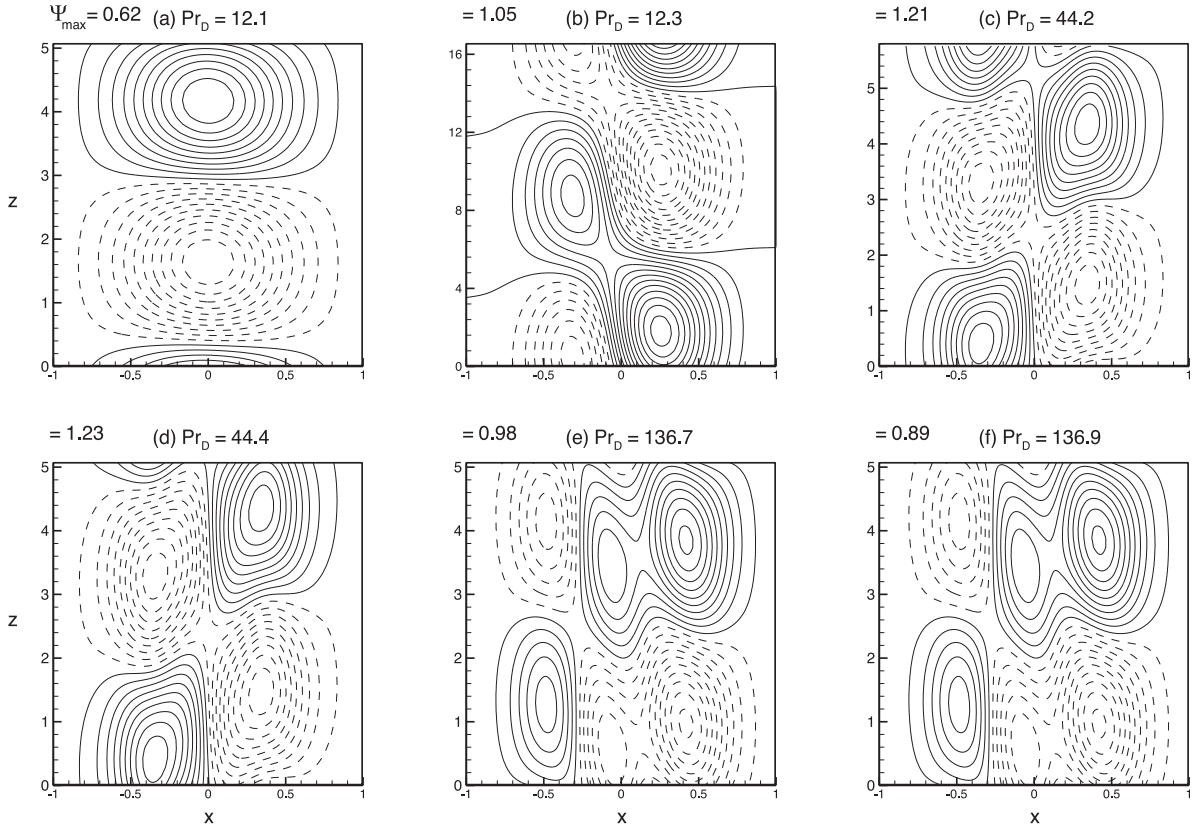

Fig. 7. The disturbance streamlines at $\sqrt{Da^{-1}}=1=M$ and $R_{eaD}=50$ for different values of Pr_D.

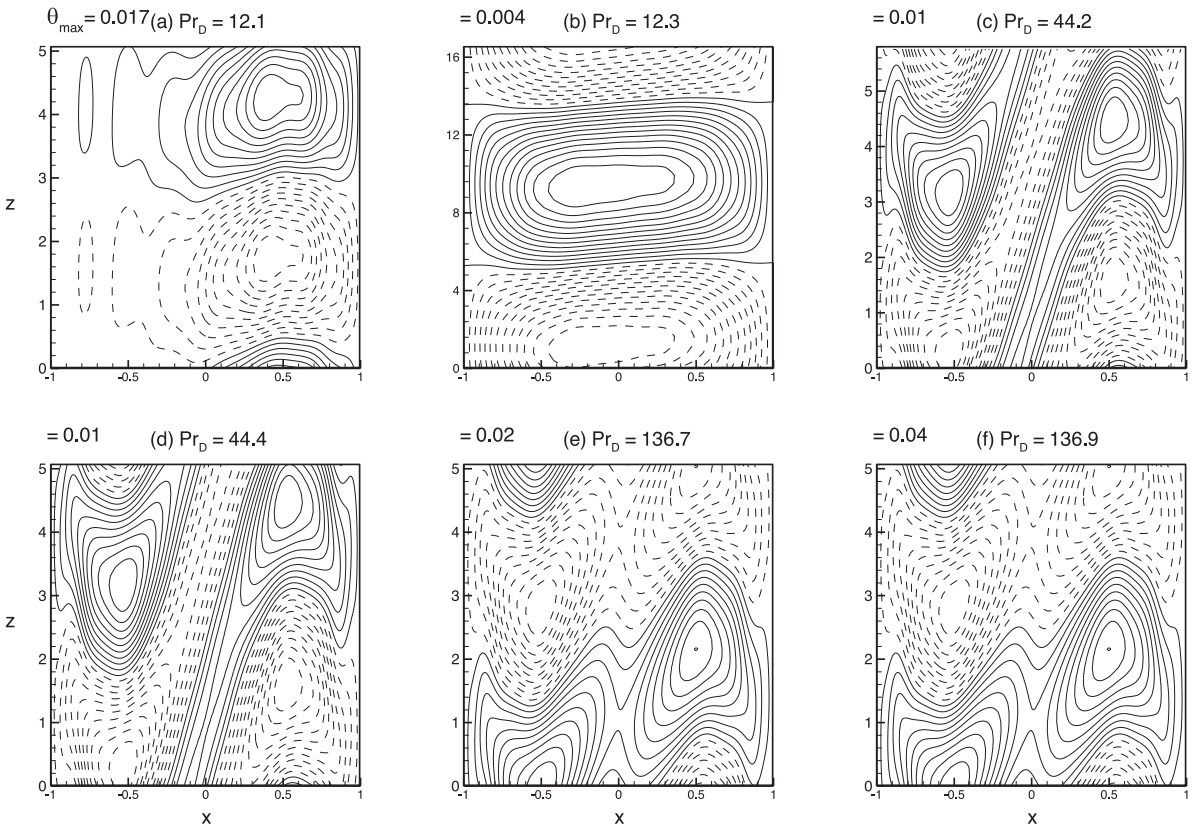

Fig. 8. The disturbance isotherms at $\sqrt{Da^{-1}} = 1 = M$ and $R_{eaD} = 50$ for different values of Pr_D.

Table 4
Variation of R_{Dc} and energy spectrum as a function of Pr_D and $\sqrt{Da^{-1}}$ at $R_{eaD}=50$ and $M=1$.

$\sqrt{Da^{-1}}$	Pr_D	R_{Dc}	E_s	E_D	E_d	E_b	E_e
0.5	3.0	49804.572790	0.784256	−0.014264	−1.000000	0.230173	0.000096
	3.1	51466.316779	0.783093	−0.014249	−1.000000	0.231324	0.000093
	3.2	42787.295581	0.014915	−0.021193	−0.993746	1.000000	0.000073
	10.0	26789.475313	−0.011729	−0.023020	−0.965386	1.000000	0.000167
	20.0	35368.893697	−0.006657	−0.023314	−0.970099	1.000000	0.000091
	50.0	55356.729218	−0.004804	−0.022999	−0.972232	1.000000	0.000045
1.0	3.0	3614.991416	0.865652	−0.058229	−1.000000	0.192367	0.001455
	10.0	12102.045597	0.806516	−0.055751	−1.000000	0.250012	0.000410
	12.2	14769.039233	0.798545	−0.055364	−1.000000	0.257663	0.000333
	12.3	12927.360435	0.007679	−0.077779	−0.929928	1.000000	0.000220
	20.0	6977.095337	−0.013651	−0.082561	−0.904309	1.000000	0.000691
	50.0	8161.211361	−0.011871	−0.085378	−0.903139	1.000000	0.000493
2.0	3.0	390.343298	1.000000	−0.209133	−0.947373	0.142590	0.015321
	10.0	1312.208594	0.937712	−0.211236	−1.000000	0.270466	0.004415
	20.0	2642.093549	0.886753	−0.204194	−1.000000	0.316662	0.002093
	44.3	5871.486993	0.838016	−0.196468	−1.000000	0.358812	0.000896
	44.4	5741.526922	−0.021873	−0.231796	−0.746564	1.000000	0.000389
	50.0	3628.722121	−0.026603	−0.237509	−0.736670	1.000000	0.000937

istics as noted above before and after the threshold value of Pr_D. Thermal energy spectrums show that disturbance thermal energy due to thermal convection (T_c) has a destabilizing effect on the flow and disturbance thermal energy due to diffusion effect (T_d) has a stabilizing effect throughout the domain of Pr_D (Figs. 10(b), 11(b) and 12(b)) for all three values of Da^{-1} considered here. As can be seen from Table 4, similar to the results of Su and Chung [44], kinetic disturbances lose their energy to the mean flow by the shear destruction (E_s) when Pr_D crosses the threshold value for all the three values of Da^{-1}. However, the characteristics of E_s is a function of Pr_D and energy is gained from the mean flow when Pr_D is less than the threshold value for a given set of parameters.

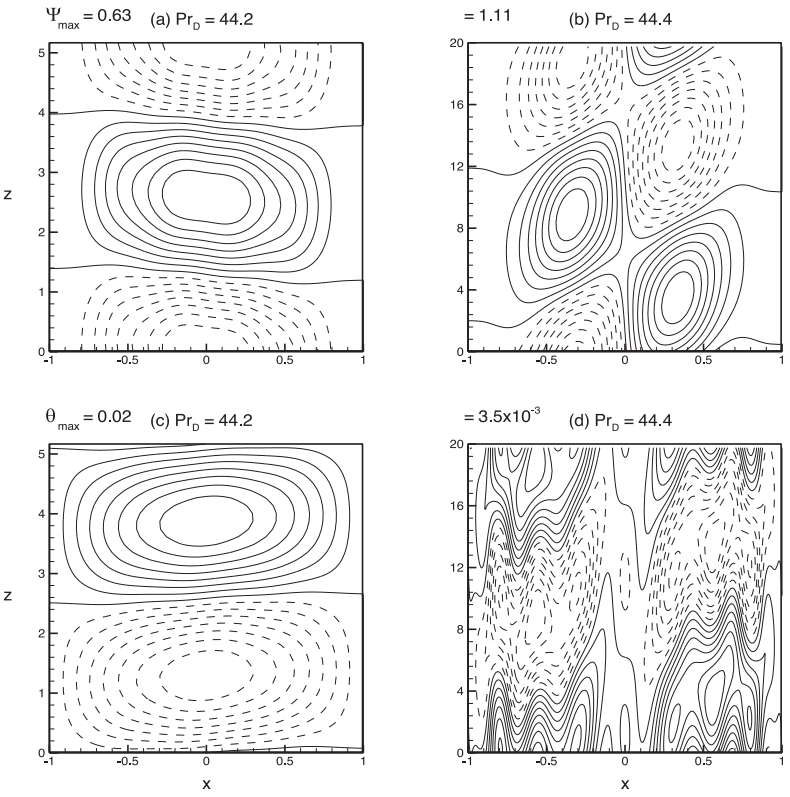

Fig. 9. The disturbance streamlines (a, b) and isotherms (c,d) at $\sqrt{Da^{-1}} = 2$, $M = 1$ and $R_{eaD} = 50$ for different values of Pr_D.

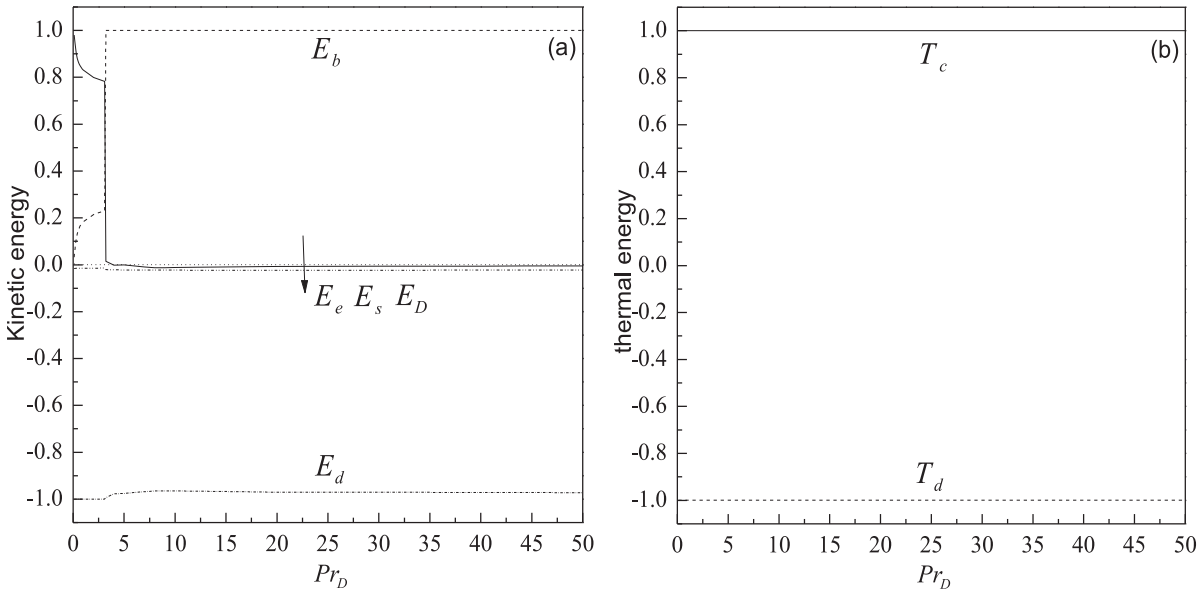

Fig. 10. The rate of change of (a) kinetic energy and (b) thermal energy as a function of Pr_D for $\sqrt{Da^{-1}} = 0.5$, $M = 1$ and $R_{eaD} = 50$.

The variation of R_{Dc} and a_c with Pr_D is shown in Fig. 13(a) and (b) for a fixed value of $Da^{-1} = 16$ with $M = 1$ and for different values of R_{eaD}. For a fixed value of R_{eaD}, it is observed that R_{Dc} increases linearly with Pr_D till $Pr_D < 136.8$ and exceeding which R_{Dc} decreases monotonically. Although the effect of increasing R_{eaD} is to instill instability on the system but its influence is found to be not so significant (Fig. 13(a) and Table 5). That is, higher the AC electric field strength the less stable the system due to an increase in the destabilizing electrostatic energy to the system. If the disturbances are

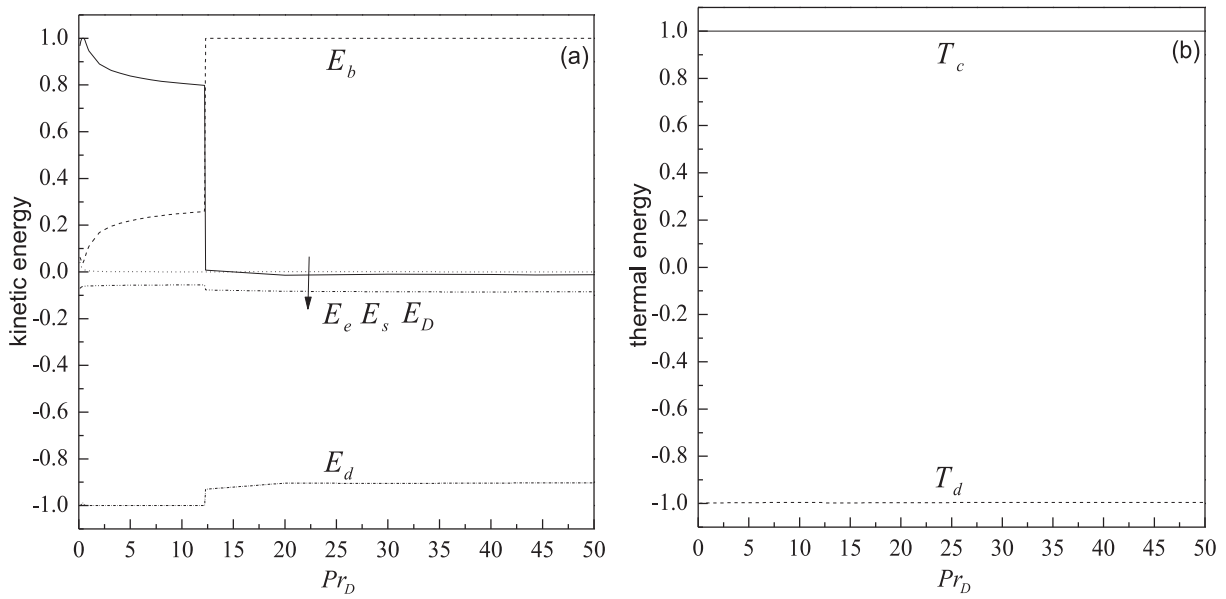

Fig. 11. The rate of change of (a) kinetic energy and (b) thermal energy as a function of Pr_D for $\sqrt{Da^{-1}} = 1 = M$ and $R_{eaD} = 50$.

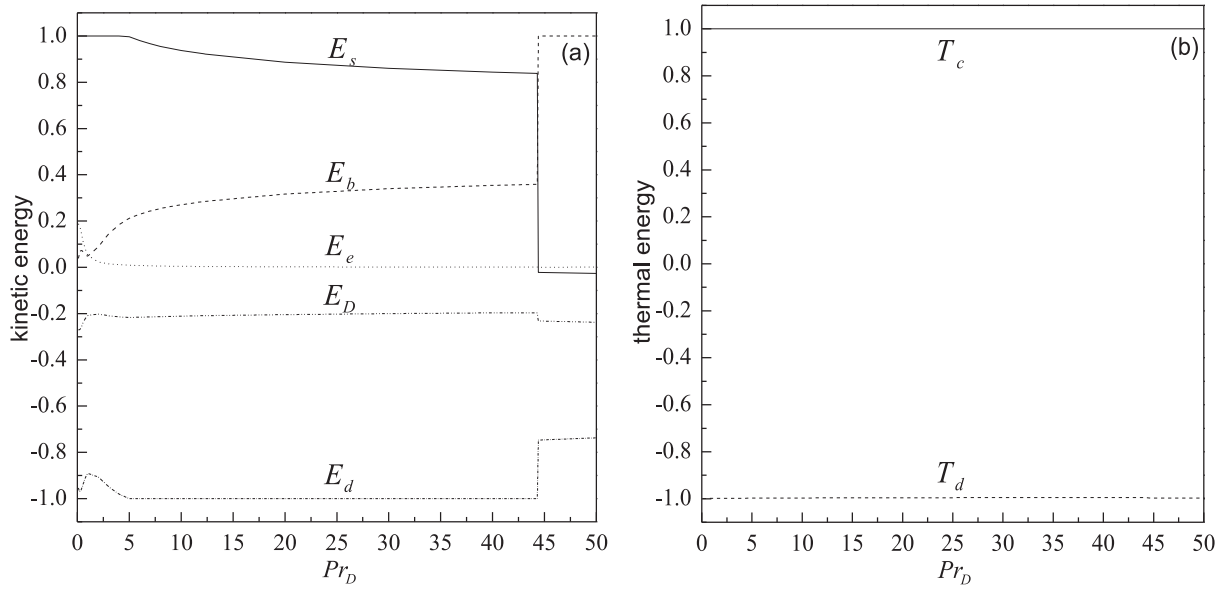

Fig. 12. The rate of change of (a) kinetic energy and (b) thermal energy as a function of Pr_D for $\sqrt{Da^{-1}} = 2$, $M = 1$ and $R_{eaD} = 50$.

Table 5
Variation of R_{Dc} as a function of R_{eaD} and Pr_D for $\sqrt{Da^{-1}} = 4$ and $M = 1$.

Pr_D	$R_{eaD} = 0$ R_{Dc}	$R_{eaD} = 50$ R_{Dc}	$R_{eaD} = 70$ R_{Dc}
1	45.738381	30.694852	21.3412548
5	265.299459	254.972191	250.596912
10	533.833851	523.163845	518.760672
20	1084.409239	1074.239751	1070.111057
50	2722.912919	2713.021507	2709.043272
100	5451.337417	5441.506959	5437.561758
136.8	7455.751171	7445.955952	7442.029549
136.9	6747.693963	6738.556048	6733.486613
150	3918.709473	3912.694057	3910.936924
200	2105.444243	2091.925569	2086.514911

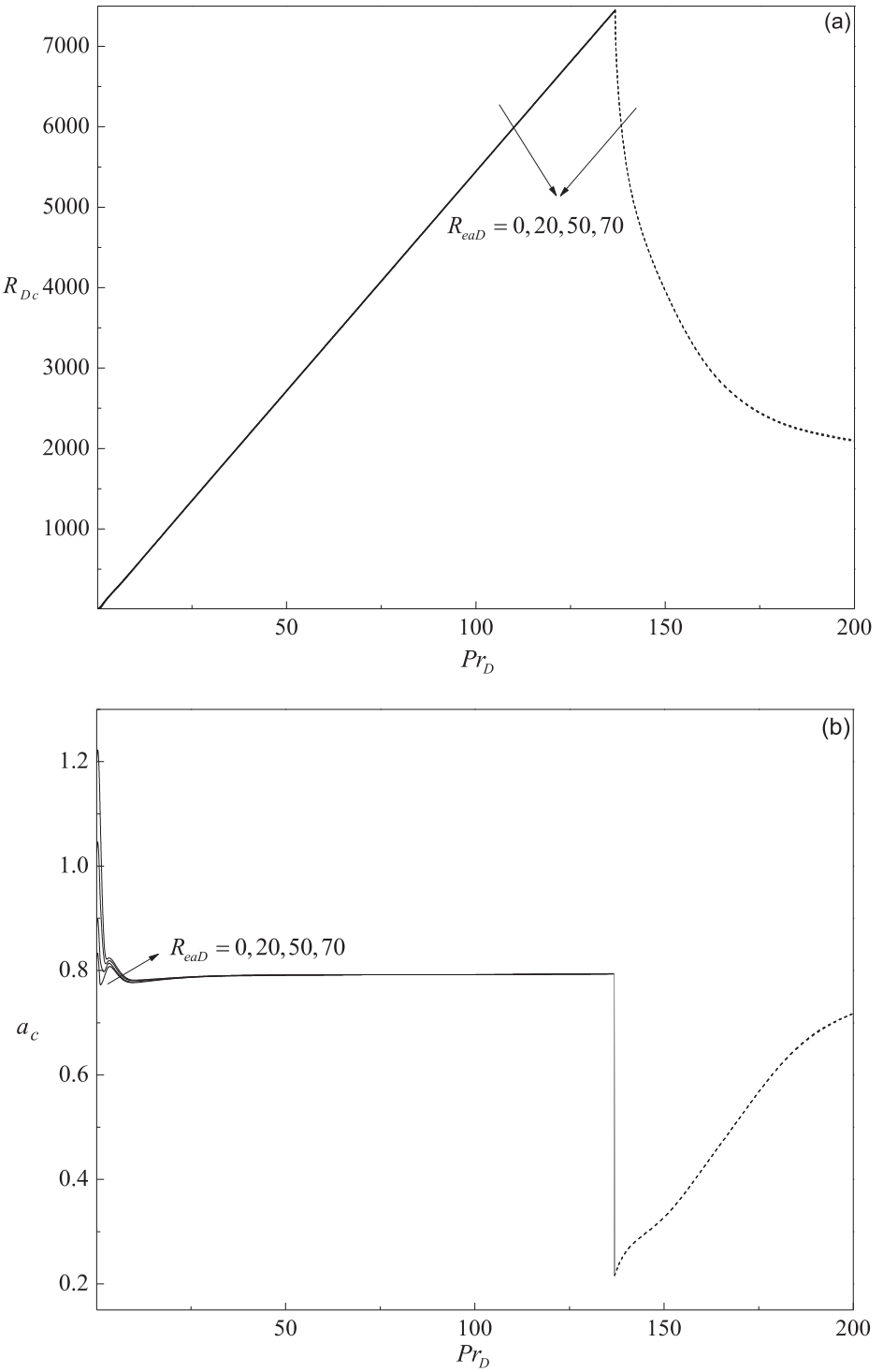

Fig. 13. Variation of (a) critical Darcy–Rayleigh number R_{Dc}, (b) critical wave number a_c and (c) critical wave speed c_c with the Darcy–Prandtl number Pr_D for a fixed value of $\sqrt{Da^{-1}} = 4$, $M = 1$ and for various values of R_{eaD}. (——) Stationary modes, (.....) travelling-wave modes.

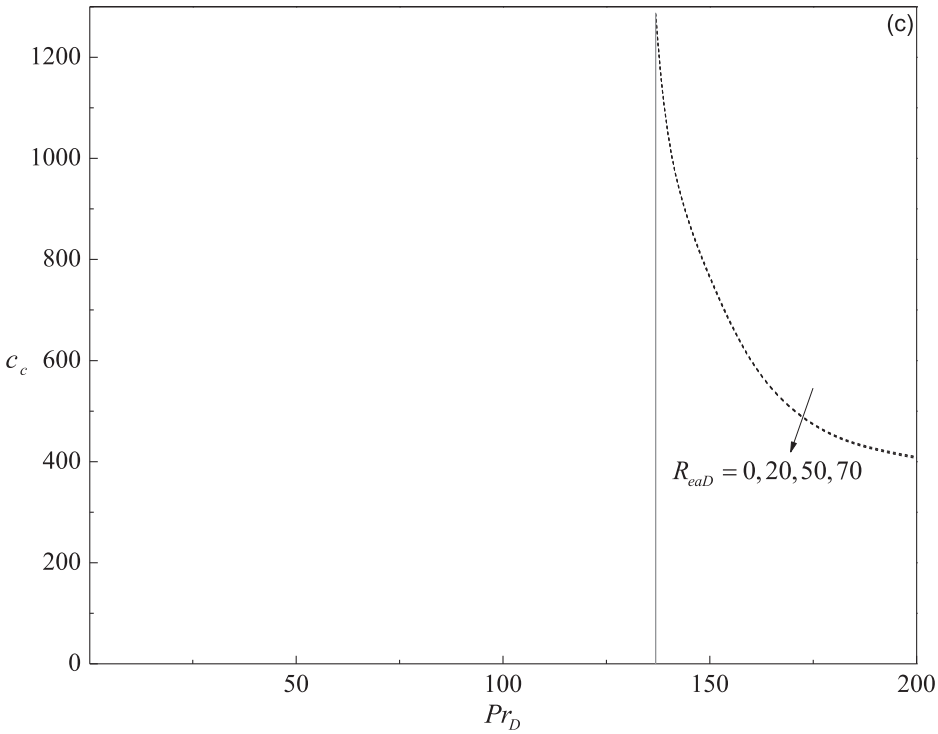

Fig. 13. Continued

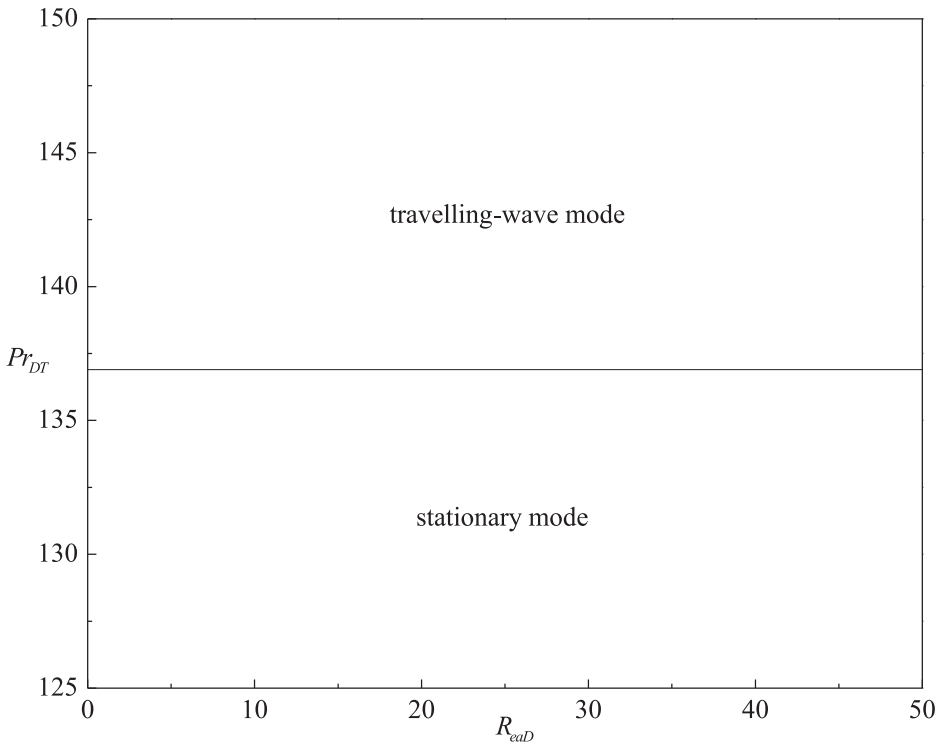

Fig. 14. Variation of Pr_{DT} (transition Darcy–Prandtl number at the critical domains) as a function of R_{eaD} when $\sqrt{Da^{-1}} = 4$, $M = 1$.

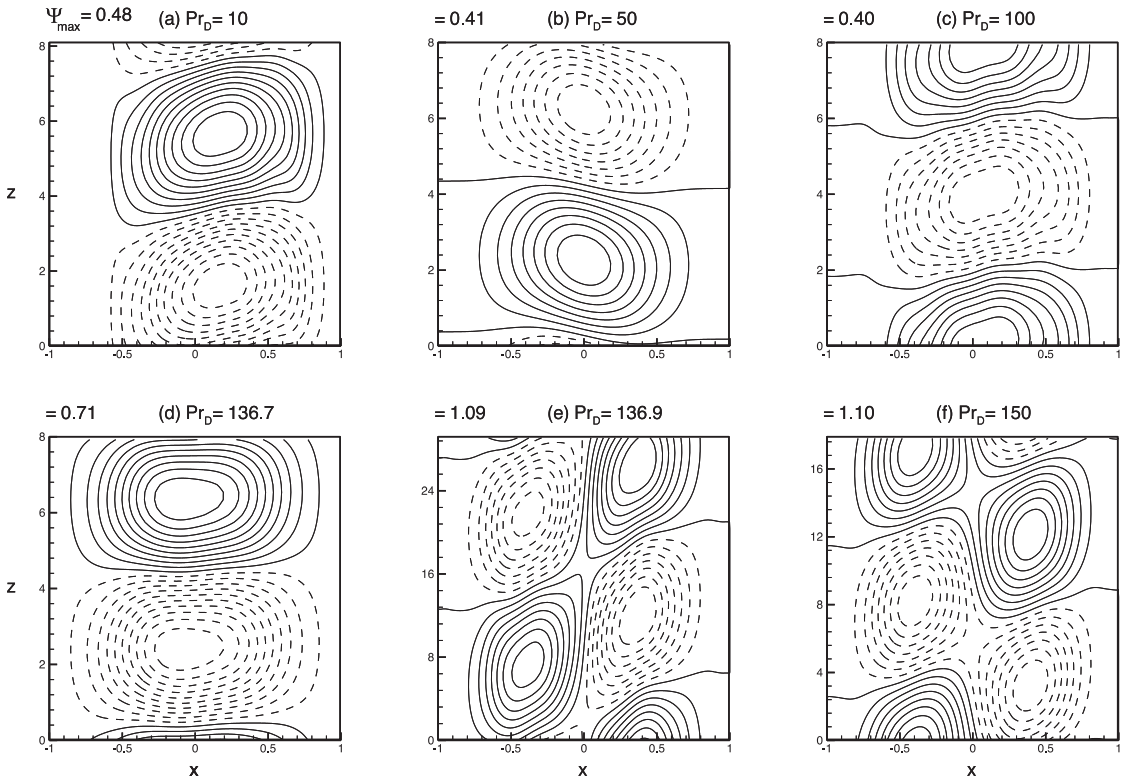

Fig. 15. The disturbance streamlines at $R_{eaD} = 0$, $M = 1$ and $\sqrt{Da^{-1}} = 4$ for different values of Pr_D.

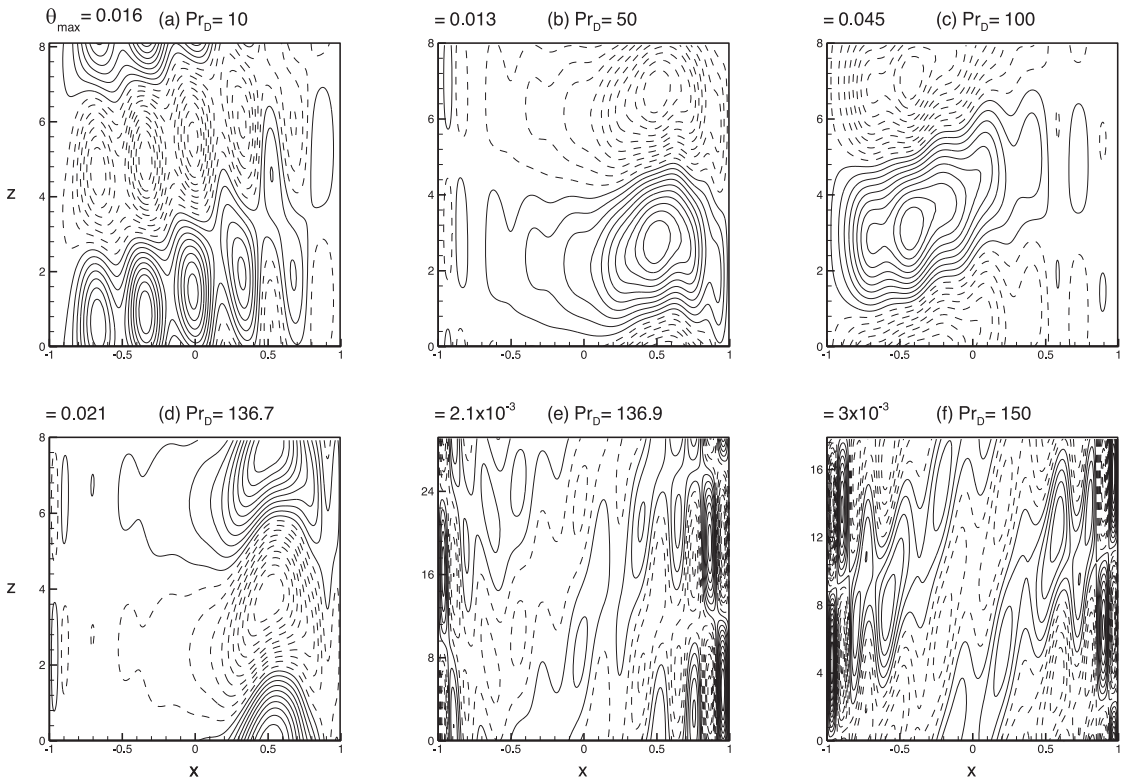

Fig. 16. The disturbance isotherms at $R_{eaD} = 0$, $M = 1$ and $\sqrt{Da^{-1}} = 4$ for different values of Pr_D.

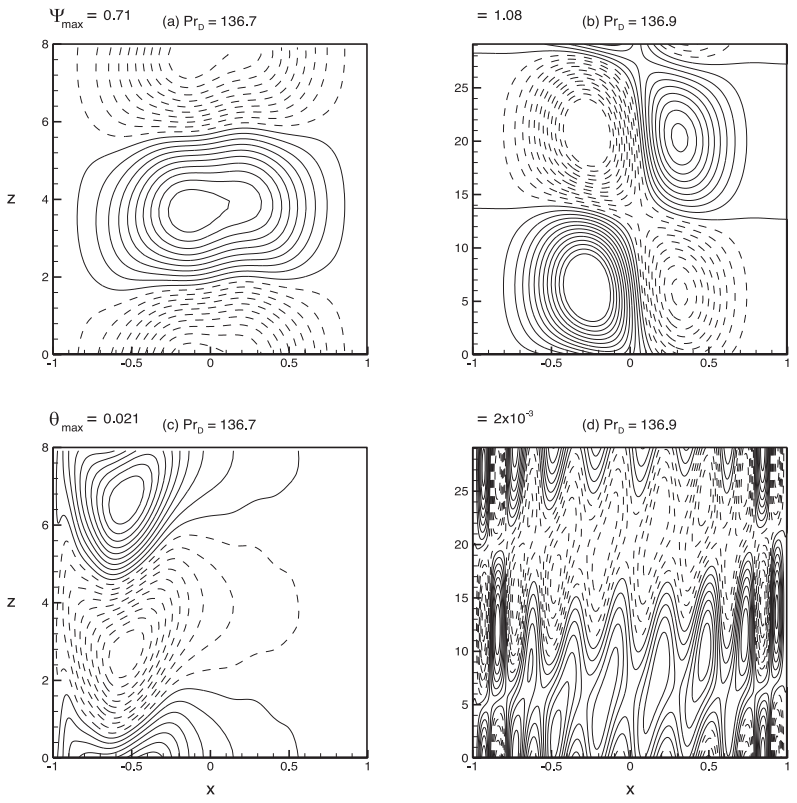

Fig. 17. The disturbance streamlines (a, b) and isotherms (c,d) at $R_{eaD} = 50$, $M = 1$ and $\sqrt{Da^{-1}} = 4$ for different values of Pr_D.

stationary, dependence of the critical wave number a_c on Pr_D is very weak while a_c at travelling-wave mode is an increasing function of Pr_D. The vertical line represents the discontinuous changes in a_c due to transition from stationary to travelling-wave mode (Fig. 13(b)) and this behavior is unaltered with increasing R_{eaD}. Fascinatingly, the value of Pr_D at which transition from stationary to travelling-wave instability occurs remain invariant for all the values of R_{eaD} considered. This aspect has been clearly shown in Fig. 14. Additional information regarding the nature of the travelling-wave mode instability can be obtained from Fig. 13(c), which shows the variation of positive c_c with Pr_D for various values of R_{eaD} when $Da^{-1} = 16$ and $M = 1$. In this figure, the vertical lines represent the discontinuous changes in c_c due to the transition from stationary to travelling-wave mode. Also, it is observed that c_c for the travelling-wave mode is a monotonically decreasing function of Pr_D. The variation of R_{eaD} on c_c is found to be not so significant.

As in the previous case, the streamlines and isotherms at the critical state for both stationary and travelling-wave modes are analyzed for this case as well. Figs. 15 and 16 show the results for different values of Pr_D and for a fixed value of $R_{eaD} = 0$ and $Da^{-1} = 16$. From Figs. 15(a) and 16(a) it can be seen that for $Pr_D = 10$, the flow pattern appears to be as stationary uni-cellular in streamlines (Fig. 15(a)) and a flurry of activity is noticed in isotherms i.e., cells of various patterns and shapes are seen throughout the spread of porous layer (Fig. 16(a)). When $Pr_D = 50$, 100 and 136.7, it is observed that the convective motion is uni-cellular (Fig. 15(b)–(d)) but the corresponding isotherms reveal that the undulation observed in Fig. 16(b) and (c) seem concentrated towards the hot wall (Fig. 16(b))/cold wall (Fig. 16(c)) followed by relatively milder formation at the cold wall (Fig. 16(b))/hot wall (Fig. 16(c)). Fig. 16(d) portrays a case of vigorous convection in the cell formation towards the colder end, followed by a lull towards the warmer side. The instability switches over from stationary to travelling-wave mode once the value of Pr_D exceeds 136.7. When $Pr_D = 136.9$, convective cells change from uni-cellular to bi-cellular in streamlines (Fig. 15(e)). Also, shapes of the isotherms appear to be multi-cellular and distributed throughout the porous layer being sparser at the middle and getting denser towards at the ends (Fig. 16(e)). It is further seen that the actual wavelengths are substantially larger in both streamlines and isotherms and at this stage, $\Psi_{\max}$, increases from 0.71 to 1.09 and $\theta_{\max}$ decreases from 0.021 to 0.002. This fact is evident from Figs. 15(e) and 16(e). It is observed that qualitatively and quantitatively the flow strength remains almost the same in both streamlines and isotherms as Pr_D increases to 150 (Figs. 15(f) and 16(f)). Interestingly, secondary flow behavior remains invariant for all the values of R_{eaD} considered. The change in streamlines and isotherms patterns is found to remain unaltered with increasing value of R_{eaD}. This fact is evident from Fig. 17 in which the results are presented for $R_{eaD} = 50$.

The energy analysis at the critical state has also been carried out as explained previously. For the above case, the threshold value of Pr_D at which the change of mode takes place is 136.8. To understand the characteristics of neural stability,

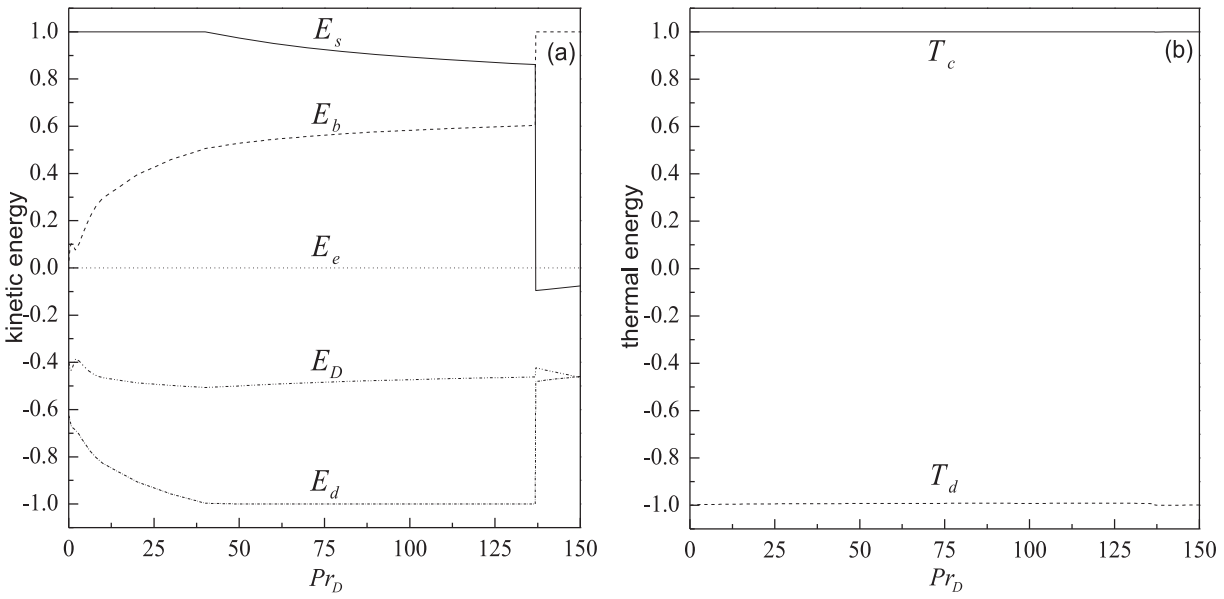

Fig. 18. The rate of change of (a) kinetic energy and (b) thermal energy as a function of Pr_D for $R_{eaD}=0$, $M=1$ and $\sqrt{Da^{-1}}=4$.

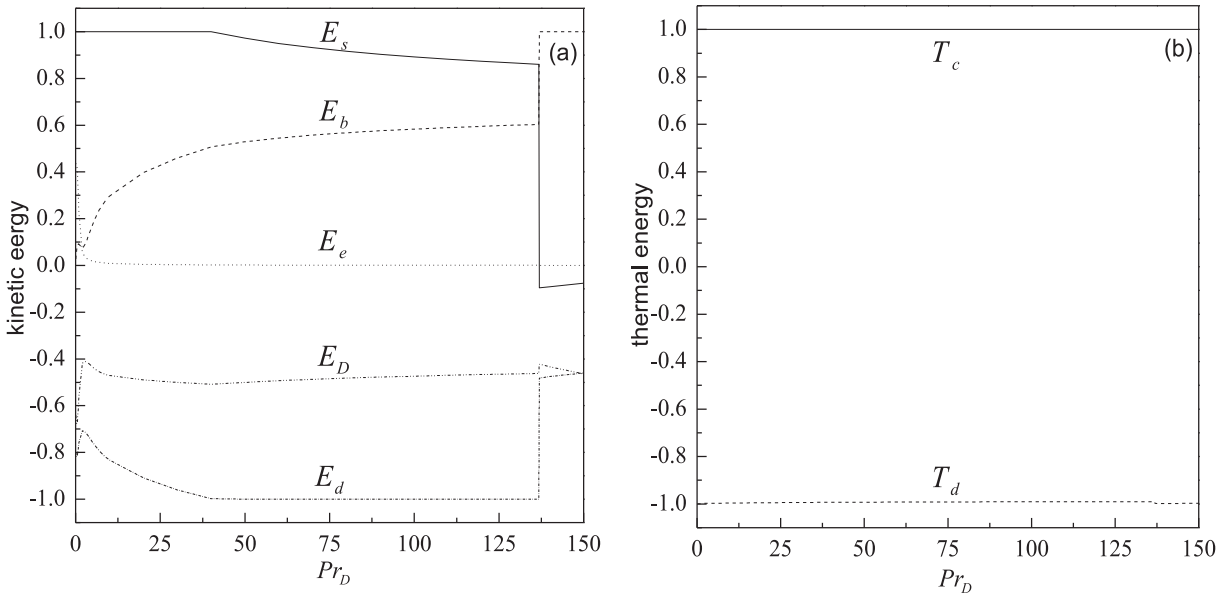

Fig. 19. The rate of change of (a) kinetic energy and (b) thermal energy as a function of Pr_D for $R_{eaD}=50$, $M=1$ and $\sqrt{Da^{-1}}=4$.

kinetic energy spectrums are analyzed as a function of Pr_D for three different values of $R_{eaD}=0$, 50 and 70 (see Figs. 18–20). From the figures it is evident that the energy spectrums show same behavior as a function of Pr_D for all the values of R_{eaD}. It is also seen that the kinetic energy spectrum profile is independent of the value of R_{eaD} and show the same characteristics before and after the threshold value of Pr_D (= 136.8) as discussed earlier.

7. Conclusions

The linear instability of natural convection in a vertical dielectric fluid saturated Brinkman porous layer under the influence of a uniform horizontal AC electric field is investigated. Coupled stability equations are solved numerically using the Chebyshev collocation method. The effect of Darcy number, Darcy–Prandtl number and AC electric Darcy-Rayleigh number on the instability characteristics of the system is delineated. The basic stationary and parallel flow is not influenced by the AC electric field while the Darcy number alters it significantly. Despite the presence of AC electric field, the basic flow is found to be stable in the absence of inertia. Nonetheless, the inclusion of inertia causes instability in the system and the

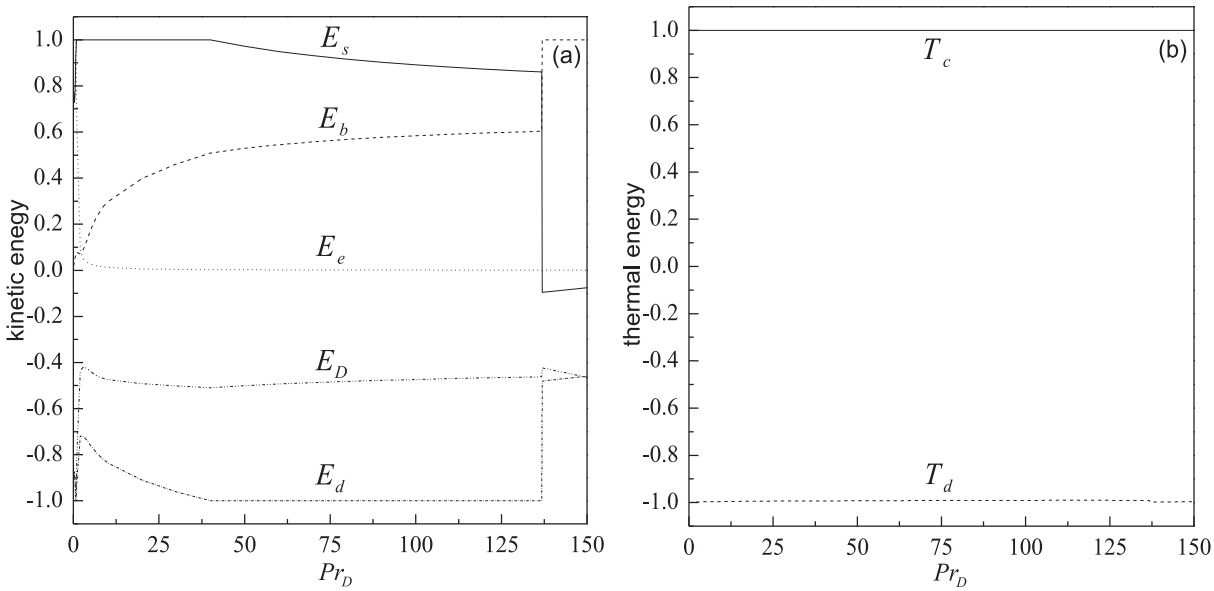

Fig. 20. The rate of change of (a) kinetic energy and (b) thermal energy as a function of Pr_D for $R_{eaD}=70$, $M=1$ and $\sqrt{Da^{-1}}=4$.

value of modified Darcy–Prandtl number at which the transition occurs from the stationary to travelling-wave mode instability increases with increasing Darcy number but remains invariant with varying AC electric Darcy–Rayleigh number. If the instability is via stationary mode the effect of Darcy number is found to be destabilizing while it exhibits a dual behavior if the instability is via travelling-wave mode. The streamlines and isotherms presented mimic the behavior of stability curves observed before and after the change of mode of instability. The dissipation of disturbance kinetic energy due to surface drag, viscous force and non-uniform electric field show no significant contribution on the stability of the flow. But the disturbance thermal energy due to convection and diffusion shows destabilizing and stabilizing tendencies, respectively. More importantly, the production of kinetic energy due to shear term diminishes drastically as the Darcy–Prandtl number crosses its threshold value, which could be associated to the change of stationary to travelling-wave mode of secondary flow. Also the kinetic energy production is almost balanced by energy dissipation due to viscous term in the entire domain of Darcy–Prandtl number.

Acknowledgments

We thank the anonymous reviewers for their helpful suggestions which helped in improving the paper considerably. One of the authors B.M.S wishes to thank the authorities of his University for their encouragement and support.

References

[1] D.A. Nield, A. Bejan, Convection in Porous Media, 4th edn., Springer, New York, 2013.
[2] B. Straughan, The Energy Method, Stability, and Non-linear Convection, Springer, New York, 2004.
[3] B. Straughan, Stability and Wave Motion in Porous Media, Springer, New York, 2008.
[4] A.E. Gill, A proof that convection in a porous vertical slab is stable, J. Fluid Mech. 35 (1969) 545–547.
[5] L.P. Kwok, C.F. Chen, Stability of thermal convection in a vertical porous layer, ASME J. Heat Trans 109 (1987) 889–893.
[6] Y. Qin, P.N. Kaloni, A nonlinear stability problem of convection in a porous vertical slab, Phys Fluids A 5 (1993) 2067–2069.
[7] M.J.S. de Lemos, Turbulence in Porous Media: Modeling and Applications, Elsevier, 2012.
[8] A. Barletta, A proof that convection in a porous vertical slab may be unstable, J. Fluid Mech. 770 (2015) 273–288.
[9] A. Barletta, Instability of stationary two-dimensional mixed convection across a vertical porous layer, Phy. Fluids 28 (2016) 014101-1-14.
[10] D.A.S. Rees, The effect of local thermal nonequilibrium on the stability of convection in a vertical porous channel, Transp. Porous Media 87 (2011) 459–464.
[11] N.L. Scott, B. Straughan, A nonlinear stability analysis of convection in a porous vertical channel including local thermal nonequilibrium, J. Math. Fluid Mech. 15 (2013) 171–178.
[12] B.M. Shankar, I.S. Shivakumara, On the stability of natural convection in a porous vertical slab saturated with an Oldroyd-B fluid, Theor. Comput. Fluid Dyn. (2016), doi:10.1007/s00162-016-0415-8.
[13] B.M. Shankar, I.S. Shivakumara, Effect of local thermal nonequilibrium on the stability of natural convection in an Oldroyd-B fluid saturated vertical porous layer, ASME J. Heat Transf. 139 (2017) 041001-1-10.
[14] B.M. Shankar, J. Kumar, I.S. Shivakumara, Stability of natural convection in a vertical layer of Brinkman porous medium, Acta Mech 228 (2017) 1–19.
[15] B.M. Shankar, J. Kumar, I.S. Shivakumara, Boundary and inertia effects on the stability of natural convection in a vertical layer of an anisotropic Lapwood–Brinkman porous medium, Acta Mech (2017), doi:10.1007/s00707-017-1831-6.
[16] N. Rudraiah, Linear and non-linear magnetoconvection in a porous medium, Proc. Indian Acad. Sci. 93 (1984) 117–135.
[17] S. Alchaar, P. Vasseur, E. Bilgen, Effect of a magnetic field on the onset of convection in a porous medium, Heat Mass Transf. 30 (1995) 259–267.
[18] M.I. Bergman, D.R. Fearn, J. Bloxham, Suppression of channel convection in solidifying Pb–Sn alloys via an applied magnetic field, Metall Mat. Trans. A 30 (1999) 1809–1815.

[19] M.S. Muddamallappa, D. Bhatta, D.N. Riahi, Numerical investigation on marginal stability and convection with and without magnetic field in a mushy layer, Transp. Porous Med. 79 (2009) 301–317.
[20] D. Bhatta, M.S. Muddamallappa, D.N. Riahi, On perturbation and marginal stability analysis of magnetoconvection in active mushy layer, Transp. Porous Med. 82 (2010) 385–399.
[21] D.N. Riahi, On magneto convection in a mushy Layer, Trans. Porous Med. 89 (2011) 285–286.
[22] O.D. Makinde, Magneto-hydrodynamic stability of plane-poiseuille flow using multideck asymptotic technique, Math. Comp. Model. 37 (2003) 251–259.
[23] O.D. Makinde, P.Y. Mhone, Temporal stability of small disturbances in MHD Jeffery–Hamel flows, Comp. Math Appl. 53 (2007) 128–136.
[24] O.D. Makinde, P.Y. Mhone, On temporal stability analysis for hydromagnetic flow in a channel filled with a saturated porous medium, Flow Turbul. Combust. 83 (2009) 21–32.
[25] B.M. Shankar, J. Kumar, I.S. Shivakumara, Magnetohydrodynamic stability of natural convection in a vertical porous slab, J. Magn. Mater. 421 (2017) 152–164.
[26] R.Z. Moreno, E.J. Bonet, O.V. Trevisan, Electric alternating current effects on flow of oil and water in porous media, in: K. Vafai, P.N. Shivakumar (Eds.), Proceeding of the International Conference Porous Media and their Applications in Science, Engineering and Industry, Hawaii, 1996, pp. 147–172.
[27] J.A. del Río, S. Whitaker, Electrohydrodynamics in porous media, Transp. Porous Med. 44 (2001) 385–405.
[28] N. Rudraiah, M.S. Gayathri, Effect of thermal modulation on the onset of electrothermoconvection in a dielectric fluid saturated porous medium, ASME J. Heat Transf. 131 (2009) 101009–101015.
[29] I.S. Shivakumara, Jinho Lee, K. Vajravelu, M. Akkanagamma, Electrothermal convection in a rotating dielectric fluid layer: effect of velocity and temperature boundary conditions, Int. J. Heat Mass Transf. 55 (2012) 2984–2991.
[30] I.S. Shivakumara, M. Akkanagamma, C.O. Ng, Electrohydrodynamic instability of a rotating couple stress dielectric fluid layer, Int. J. Heat Mass Transf. 62 (2013) 761–771.
[31] M. Takashima, H. Hamabata, The stability of natural convection in a vertical layer of dielectric fluid in the presence of a horizontal ac electric field, J. Phys. Soc. Jpn. 53 (1984) 1728–1736.
[32] M. Takashima, The stability of natural convection in a vertical layer of electrically conducting fluid in the presence of a transverse magnetic fluid, Fluid Dyn. Res. 14 (1994) 121–134.
[33] A. Yabe, Y. Mori, K. Hijikata, Active heat transfer enhancement by utilizing electric fields, Ann. Rev. Heat Transf. 7 (1996) 193–244.
[34] F.C. Lai, K.W. Lai, EHD-Enhanced drying with wire electrode, Drying Tech 20 (2002) 1393–1405.
[35] L.D. Landau, E.M. Lifshitz, Electrodynamics of Continuous Media, Pergamon Press, 1960.
[36] M. Takashima, K.D. Aldridge, The stability of a horizontal layer of dielectric fluid under the simultaneous action of a vertical dc electric field and a vertical temperature gradient, Q. J. Mech. Appl. Math. 29 (1976) 71–87.
[37] P.G. Drazin, W.H. Reid, Hydrodynamic Stability, Cambridge University Press, Cambridge, UK, 2004.
[38] S.A. Orszag, Accurate solution of the Orr-Sommerfeld stability equation, J. Fluid Mech. 50 (1971) 689–703.
[39] C. Canuto, M. Hussaini, A. Quarteroni, T.A. Zang, Spectral Methods in Fluid Dynamics, Springer, New York, 1988.
[40] B.M. Shankar, Jai Kumar, I.S. Shivakumara, Stability of natural convection in a vertical couple stress fluid layer, Int. J. Heat Mass Transf. 78 (2014) 447–459.
[41] O.D. Makinde, On the Chebyshev collocation spectral approach to stability of fluid flow in a porous medium, Int. J. Numer. Meth. Fluids 59 (2009) 791–799.
[42] B.A. Singer, J.H. Ferziger, H.L. Read, Numerical simulations of transition in oscillatory plane channel flow, J. Fluid. Mech. 208 (1989) 45–66.
[43] Y.C. Chen, J.N. Chung, The linear stability of mixed convection in a vertical channel flow, J. Fluid Mech. 325 (1996) 29–51.
[44] Y.C. Su, J.N. Chung, Linear stability analysis of mixed-convection flow in a vertical pipe, J. Fluid Mech. 422 (2000) 141–166.